Journal of African Earth Sciences 218 (2024) 105382

Contents lists available at ScienceDirect

Journal of African Earth Sciences

journal homepage: www.elsevier.com/locate/jafrearsci

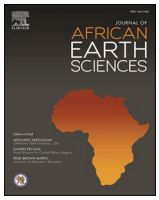

Paleostress evolution of the Outer Kwanza basin (offshore Angola); comparison with the Congo basin and implications for the tectonic history of the Central segment of the West Africa passive margin

Boubacar Bah [a], Olivier Lacombe [a,*], Nicolas E. Beaudoin [b], Pierre-Alexandre Teboul [c], Jean-Pierre Girard [b,c], Claude Gout [b,c]

[a] Sorbonne Université, Institut des Sciences de la Terre de Paris (ISTeP), CNRS-INSU, 75005, Paris, France
[b] Universite de Pau et des Pays de l'Adour, Laboratoire des Fluides Complexes et Leurs Réservoirs (LFCR), E2S UPPA, CNRS, 64000, Pau, France
[c] TotalEnergies, Centre Scientifique et Technique Jean Féger (CSTJF), 64000, Pau, France

ARTICLE INFO

Handling Editor: M Mapeo

Keywords:
Paleostress reconstruction
Calcite twinning and stylolite roughness paleopiezometry
Faults and fractures
Far-field lithospheric stress
U-Pb dating
Kwanza basin

ABSTRACT

This study aims at reconstructing the paleostress history of the Outer (offshore) Kwanza basin (West African passive margin) and at comparing it to stress results acquired further north in the Congo basin. Three oriented borehole cores provided by TotalEnergies and reaching the syn-rift, Barremian-Aptian pre-salt carbonates offshore Angola were investigated. Paleopiezometry based on the Stylolite Roughness Inversion Technique (SRIT) and Calcite Twin Inversion Technique (CSIT) was combined with fracture analysis, U–Pb geochronology of carbonates and burial modelling to unravel the orientations and magnitudes of horizontal and vertical stresses affecting the pre-salt carbonates over time. Calcite twins were measured from a primary sparite matrix, and the inversion process unravelled a polyphase stress history, comprising ~ E-W and NE-SW extensional trends that we associate to the rifting (130-112 Ma) that led to the opening of the South Atlantic ocean. The ~ E-W extension is consistent with the early occurrence of N-S striking normal faults which developed in relation to the reactivation of inherited basement structures. This ~ E-W extension evolved during the Barremian-Aptian (?) into the dominant regional NE-SW extension marked by large-scale NW-SE striking normal faults. The stress history also comprises compressional and strike-slip stress regimes associated with a ~N-S trending σ_1 which can be related to the transfer of orogenic stresses from the distant Africa-Eurasia plate boundary at ~67-60 Ma. Finally, compressional and strike-slip stress regimes associated with a ENE-WSW to ~E-W trending σ_1 dominated since at least ~17-15 Ma (possibly ~34 Ma); they are interpreted as the expression of the mid-Atlantic ridge push. These (paleo)stress results are compared and combined with earlier paleostress reconstructions in the northern offshore Lower Congo basin (also belonging to the Central segment of the margin) and in the onshore Congo basin in order to refine the stress record and the timing of tectonic events since the early Cretaceous, thus providing unprecedented constraints on the tectonic history of the West Africa passive margin. This tectonic history includes both extensional and compressional events, and was driven mainly by far-field stresses, either gravitational or tectonic in origin, which are related to interactions between the African plate and surrounding plates.

1. Introduction

Tectonic forces exerted at plate boundaries may originate from various mechanisms such as plate motions, friction between the convective mantle and the base of the lithosphere, and plume dynamics (e.g. Bott, 1993; Ziegler et al., 1995; Burov and Gerya, 2014; Koptev et al., 2018). These forces are the engines of the extensional stresses that prevail during continental rifting of the lithosphere, where local thermal and rheological heterogeneities (Cloetingh et al., 2013) enhance complexity in local and regional stress patterns.

During the protracted post-rift evolution of e.g., Atlantic-type passive margins, compressional (and extensional) tectonic stresses may have prevailed alternatively or successively from the break-up onwards. Post-rift compressional stresses may originate either from ridge push (Mahatsente, 2017) or from far-field compressional tectonic stress transfer from distant convergent plate boundaries (e.g., Ziegler et al.,

* Corresponding author.
E-mail address: olivier.lacombe@sorbonne-universite.fr (O. Lacombe).

https://doi.org/10.1016/j.jafrearsci.2024.105382
Received 17 June 2024; Received in revised form 11 August 2024; Accepted 12 August 2024
Available online 13 August 2024

1995). For instance, the recent findings by Bah et al. (2023a), Zeboudj et al. (2023) and NKodia et al. (2024) corroborated the earlier idea that the Atlantic ridge push could have controlled for long the lithospheric stress in the continental part of the African plate (Ziegler et al., 1995; Guiraud et al., 2005; Riccomini, 1995; Mahatsente and Coblentz, 2015; Medvedev, 2016; Mahatsente, 2017), with a far field transfer of compressional stress over a large distance (>2000–3000 km) from the spreading ridge. Another source of compressional stresses (and intra-plate deformation as well) is related to the far-field compressional stress transfer from distant convergent plate boundaries (Ziegler et al., 1995; Withjack et al., 1995; Vagnes et al., 1998; Viola et al., 2012; Bah et al., 2023a; Nkodia et al., 2024). Alternate stress sources also may have contributed to a lesser extent to the post-rift stress field in the Atlantic-type passive margin (Medvedev, 2016), and in passive margins in general, such as gravitational stresses arising from (1) lithosphere bending due to loading related to rapid sedimentation rates, (2) post-glacial rebound, and (3) difference in elevation and associated gravitational potential energy between the continent and the margin (Pascal, 2006; Pascal and Cloetingh, 2009). The primary control exerted by the ridge push on the present-day stress field at the Atlantic eastern passive margins is further supported by the observation that the present-day stress field is often dominated by a σ_H (i.e., the greatest horizontal principal stress) oriented roughly perpendicular to both the trend of the margin and the oceanic ridge and in a strike-slip or thrust faulting regime (e.g., World stress map, Heidbach et al., 2018).

The tectonic history of the South Atlantic passive margins is debated (Karl et al., 2013), especially considering the paleostress evolution discrepancy along each margin and between each other (Salomon et al., 2015). This debate has been updated by Zeboudj et al. (2023) and Bah et al. (2023a) who proposed new reconstructions of the paleostress fields which prevailed in the offshore Lower Congo basin from the early Cretaceous rifting event onwards. However, in offshore domains paleostress reconstructions can be carried out only thanks to cores from few deep wells sparsely distributed within the basin. Even if the results from the examined cores reveal to be consistent from one well to another, a reliable appraisal of the tectonic history of a complete segment of the West African margin before and after continental break-up requires additional investigations in neighbouring regions of the margin to check for consistency of tectonic processes in both time and space (e.g., along the strike of the margin). Additional independent information may alternatively come from onshore field tectonic studies, e.g., Viola et al. (2012) in South Africa; Salomon et al. (2015) in Namibia and more recently Nkodia et al. (2024) in the Malebo Pool in the onshore part of the Congo basin (Fig. 1).

In offshore sedimentary basins, beyond providing stratigraphic control on seismic interpretations and petroleum system characterisation, deep exploration wells drilled by oil companies offer an invaluable opportunity to collect sedimentary and burial information as well as structural data from deeply buried sedimentary formation and related reservoirs (Bah et al., 2023a, 2023b; Zeboudj et al., 2023). In carbonate sequences, mesostructures such as fractures and stylolites and microstructures such as calcite twins are the main strain markers and stress gauges (Beaudoin and Lacombe, 2018). In this paper, we aim at reconstructing the paleostress history of the Outer (offshore) Kwanza basin from three oriented borehole cores of the deeply buried Barremian-Aptian pre-salt carbonates (130-115 Ma) (Teboul, 2017). These carbonates were deposited before the widespread late Aptian salt of the Loeme Fm and therefore represent syn-rift to sag deposits (TOCA equivalent, TOCA standing for TOp CArbonates, as described in the Lower Congo basin (e.g., Grosdidier et al., 1996; Bate, 1999; Harris, 2000; Gradstein et al., 2004; Beglinger et al., 2012).

Since the TOCA Fm has proven to have recorded most of the tectonic evolution of the South Atlantic since the early Cretaceous (Bah et al., 2023a), we adopted a similar approach by combining the analysis of mechanical twins in calcite (Lacombe, 2010; Lacombe et al., 2021) and of sedimentary stylolite roughness (Beaudoin et al., 2016, 2020a, b; Labeur et al., 2021, 2024) in order to unravel both the tectonic and burial history of the pre-salt carbonates. Our study therefore provides the only paleostress constraints on the tectonic history that affected the pre-salt strata of the Outer Kwanza basin since early Cretaceous time, while most of previous work has focused on the spectacular post-rift salt-related deformation (e.g., Hudec and Jackson, 2004; Erdi and Jackson, 2021; Pichel et al., 2023). Our work complements earlier studies on the burial and paleostress history of the syn-rift pre-salt TOCA

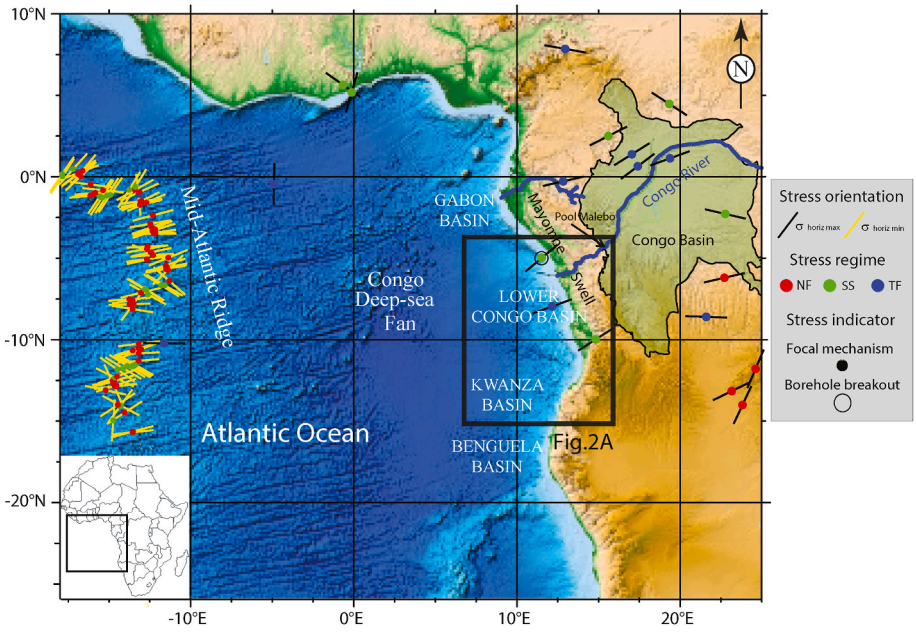

Fig. 1. General setting of the study area in the West Africa passive margin. with present-day stress indicators. Contemporary stress data from Delvaux and Barth, 2010); Heidbach et al. (2018); Nkodia et al. (2022); Bah et al. (2023a); Schirbel et al. (2024). The maximum horizontal stress (σ horiz. max) direction is represented by black bars except for the mid-Atlantic ridge where, instead, the minimum horizontal stress (σ horiz. min) direction is represented by yellow bars in order to highlight extensional trends.Topographic and bathymetric data from the Etopo1 model of the National Center for Environmental Information (NOAA), obtained from http://www.ngdc.noaa.gov/mgg/global/relief/ETOPO1/image/.

Fm (Bah et al., 2023a a,b) and of the post-rift supra-salt Sendji Fm (Zeboudj et al., 2023) in the Central segment of the West African passive margin but more to the north, in the Lower (offshore) Congo basin (Fig. 2A). The results are further compared to the paleostress history reconstructed from fault and fracture analysis in the middle Paleozoic sandstones of the Inkisi Group in the onshore Congo basin (NKodia et al., 2020, 2024), and integrated with earlier paleostress results (e.g., early Cretaceous Etendeka volcanics and Twyfelfontein sandstone in Namibia (Salomon et al., 2015) and Proterozoic metamorphic rocks in Namaqualand, western South Africa (Viola et al., 2012). Beyond yielding new information on long-recognized early Cretaceous pre-salt carbonate reservoirs, this study discusses the tectonic evolution of the West Africa passive margin though time as well as the origin of stresses (tectonic vs gravitational) that prevailed since the early Cretaceous rifting onwards, with possible implications for the dynamics of divergent passive margins worldwide.

2. Geological setting

2.1. Tectono-sedimentary setting of the central segment of the West Africa passive margin

The South Atlantic is typically divided into three segments: Equatorial, Central and Austral segments, which formed during the diachronous, northward-propagating rifting and dislocation of the supercontinent Gondwana during the late Jurassic to early Cretaceous (Mohriak et al., 2008; Matton and Jébrak, 2009; Pletsch et al., 2001; Szatmari and Milani, 2016; Heine et al., 2013; Moulin et al., 2005). These segments are bounded by NE-SW-striking transform structures and have distinct extensional and subsidence histories (Mbina Mounguengui and Guiraud, 2009).

In the Central South Atlantic, the area of focus of this contribution, rifting occurred during the early Cretaceous (ca. 143–112 Ma) under an overall NE-SW-oriented extension and was followed by continental breakup between the South American and African plates, creating the conjugate continental margins of West Africa and East Brazil (Rabinowitz and LaBrecque, 1979; Moulin et al., 2010; Chaboureau et al., 2013; Heine et al., 2013; Kukla et al., 2018). The West African central segment is composed of three main sedimentary basins, namely the Gabon, Lower Congo and Kwanza basins (Figs. 1 and 2A).

The tectonic-sedimentary history of the Central South Atlantic segment comprises several distinctive stages. The pre-rift stage was marked by intracratonic faulting and deposition of continental clastics of Carboniferous-Jurassic age in the interior basins of Gabon and in the eastern part of the Congo basin (Teisserenc and Villemin, 1989; Brownfield and Charpentier, 2006; Delvaux et al., 2021). The onshore part of the Kwanza basin contains pre-rift rocks of potentially Jurassic age, consisting of the Red Beds and Red Basal continental strata (Burwood, 1999) but pre-rift rocks have not been reached by drilling in the offshore part of the basin (Brownfield and Charpentier, 2006). In the offshore Lower Congo basin, Jurassic rocks are seemingly absent and the early Cretaceous sequences rest directly on the Precambrian crystalline basement and overlying Precambrian sedimentary strata (Brice et al., 1982; Schoellkopf and Patterson, 2000).

The first syn-rift stage between the Berriasian and Middle Barremian (~144-127 Ma) corresponds to the development and activity of normal faults generating tilted blocks and basins (Brownfield and Charpentier, 2006) and deposition of a syn-rift, ca 2–3 km thick fluvio-continental succession in the northern domain (Beglinger et al., 2012) while the clastic sediments are thinner in the Kwanza domain (Saller et al., 2016) and even thinner on certain horst structures (Qiu et al., 2020). The second syn-rift stage, from middle Barremian to Aptian (~127-117 Ma), corresponds to a weakly faulted, ca. 1–2 km thick syn-rift sedimentary sequences (Uncini et al., 1998; Beglinger et al., 2012) which was deposited in lacustrine to shallow marine depositional environments after most of the fault activity ceased locally and rifting migrated westwards towards the future distal margin. The entire sedimentary sequence associated with these two stages of rifting is commonly referred to as "pre-salt" and/or belonging to the early "sag basin". The late syn-rift phase (transition phase) is associated with deposition of a thick, on average 2–2.5 km and locally up to 4 km, Aptian salt along most of the Central South Atlantic (Lehner and de Ruiter, 1977; Teisserenc and Villemin, 1989; Aslanian et al., 2009; Davison, 2007; Hudec and Jackson, 2004; Lentini et al., 2010; Pichel et al., 2023; Rowan, 2020) towards the end of the Aptian (117-112 Ma). The deposition of salt was probably related to progressive marine transgressions in the proto-South Atlantic (Asmus and Ponte, 1973; Beglinger et al., 2012) and to more arid conditions (Bate, 1999; Karner and Gambôa, 2007). Most of the salt was deposited prior to continental break-up and oceanic spreading and after most of crustal extension has occurred (Davison, 2007; Kukla et al., 2018; Lentini et al., 2010; Rowan, 2014).

Continental breakup started at ~112-110 Ma (Torsvik et al., 2009; Moulin et al., 2010). The salt deposits were covered by an up to ca. 1.5 km thick platform carbonate sequence and deep-water equivalents during Albian to Cenomanian times following the onset of oceanic spreading and thermal subsidence (Beglinger et al., 2012). The salt then undergoes gravity deformation when the overlying Albian carbonate platform (e.g., Sendji Fm, Zeboudj et al., 2023) began to develop significantly. This gravity deformation was achieved in three stages: (1) the initiation of salt diapirs during the lower Albian, (2) the formation of local raft structures (i.e., extensional thin-skinned units detached on a salt level) bounded by listric faults (Rouby et al., 2002; Wonham et al., 2010) and (3) the development of N-S listric normal faults. From the Cenomanian to the Eocene, sedimentation was dominated by siliciclastic progradation and/or aggradation (Anka et al., 2009; Baudouy and Legorjus, 1991; Séranne and Anka, 2005; Torsvik et al., 2009). A phase of uplift-erosion affected the sedimentary sequence by (late Eocene-) early Oligocene times (Anka et al., 2009; Hudec and Jackson, 2004) and a new prograding system was established since the Miocene coevally with the development of the Zaire depocenter. Volumes and rates of sedimentation, as well as flexural subsidence therefore varied significantly along the strike of the Central segment during the Tertiary, owing to variable distribution of sediment pathways, especially in the Congo and Kwanza fan deltas and to the Oligocene differential continental uplift and erosion (Hudec and Jackson, 2004; Marton et al., 2000; Pichel et al., 2023; Jackson and Hudec, 2009).

2.2. Stratigraphic framework of the Outer Kwanza basin

The southern portion of the Outer Kwanza basin features a volcanic seamount trend delineating its boundary with the Benguela basin (Guiraud et al., 2010). Geochronological analysis using 40Ar/39Ar dating of plagioclase minerals has identified two distinct magmatic episodes. The first episode, occurring 132 Ma ago during the Hauterivian stage, produced a significant volume of picritic basalts, tholeiitic and transitional basalts, rhyodacites, and dykes (Comin-Chiaramonti et al., 2011; Marzoli et al., 1999). This age suggests that this volcanism represents the northeastern extension of the Paraná-Angola-Etendeka continental flood province (Marzoli et al., 1999). The second magmatic episode, characterized by tholeiitic magmatism manifested in coast-parallel dykes, has been dated to 126.1 ± 1.4 Ma during the Barremian stage (Marzoli et al., 1999). These dykes intrude the basement and share similarities with other dyke swarms (such as Florianopolis, Santos-Rio de Janeiro, and Horingbaai), possibly indicating a connection to the rifting and opening of the South Atlantic (Marzoli et al., 1999).

The overall stratigraphic framework has been synthetized by Brownfield and Charpentier (2006; Fig. 3). A biostratigraphic study conducted by Bate et al. (2001) focused on non-marine ostracods and palynomorphs, as illustrated in Fig. 3, assigning the synrift sequence of the Kwanza basin to the Neocomian (Berriasian to Hauterivian) stage. The authors further divided the basin into two primary

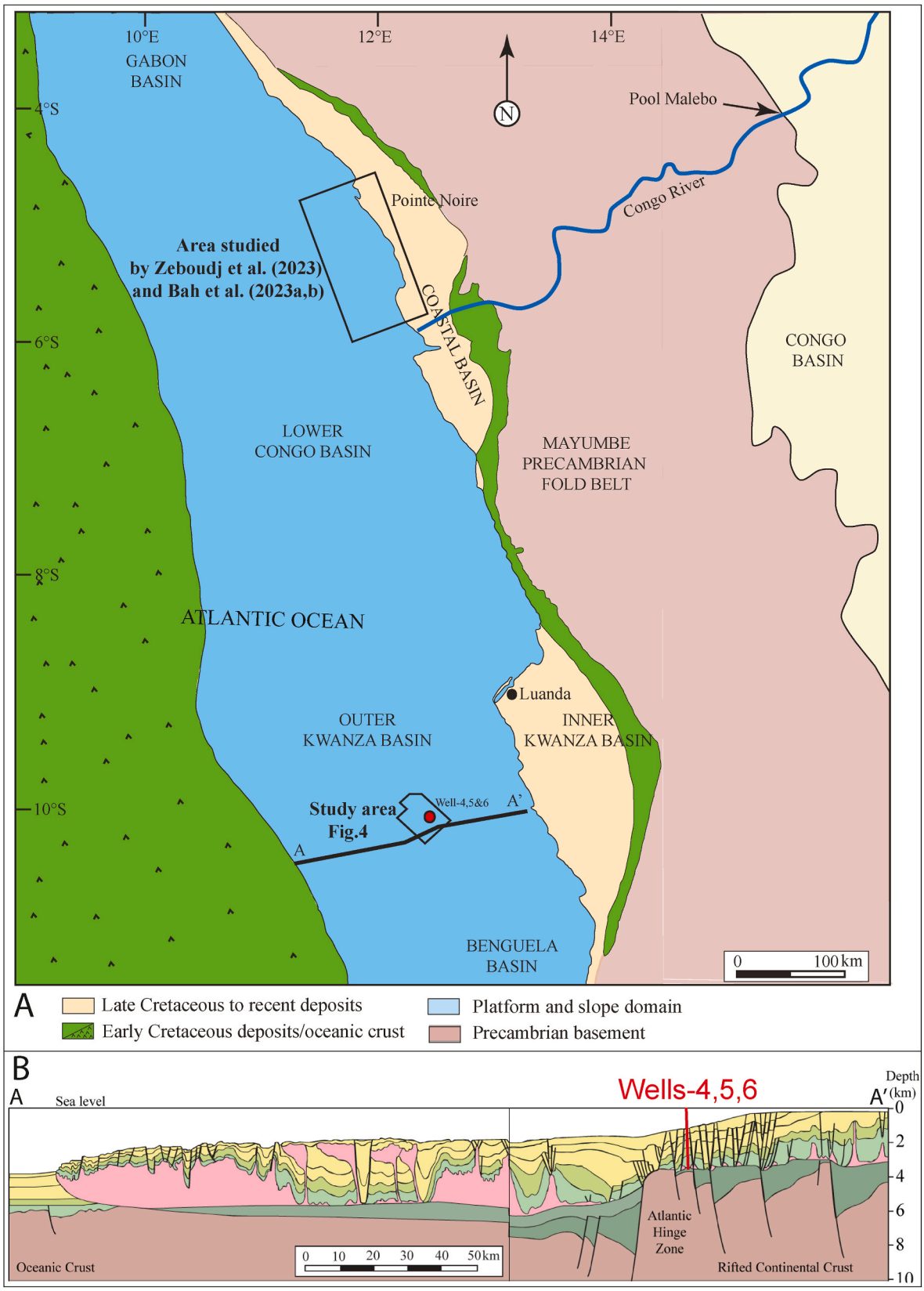

Fig. 2. A. Simplified structural map of onshore-offshore West Africa from Gabon to Angola with location of Congo and Kwanza basins. B. Geological section (modified after Erdi and Jackson, 2021) across the Kwanza basin, with approximate projection of the studied wells.

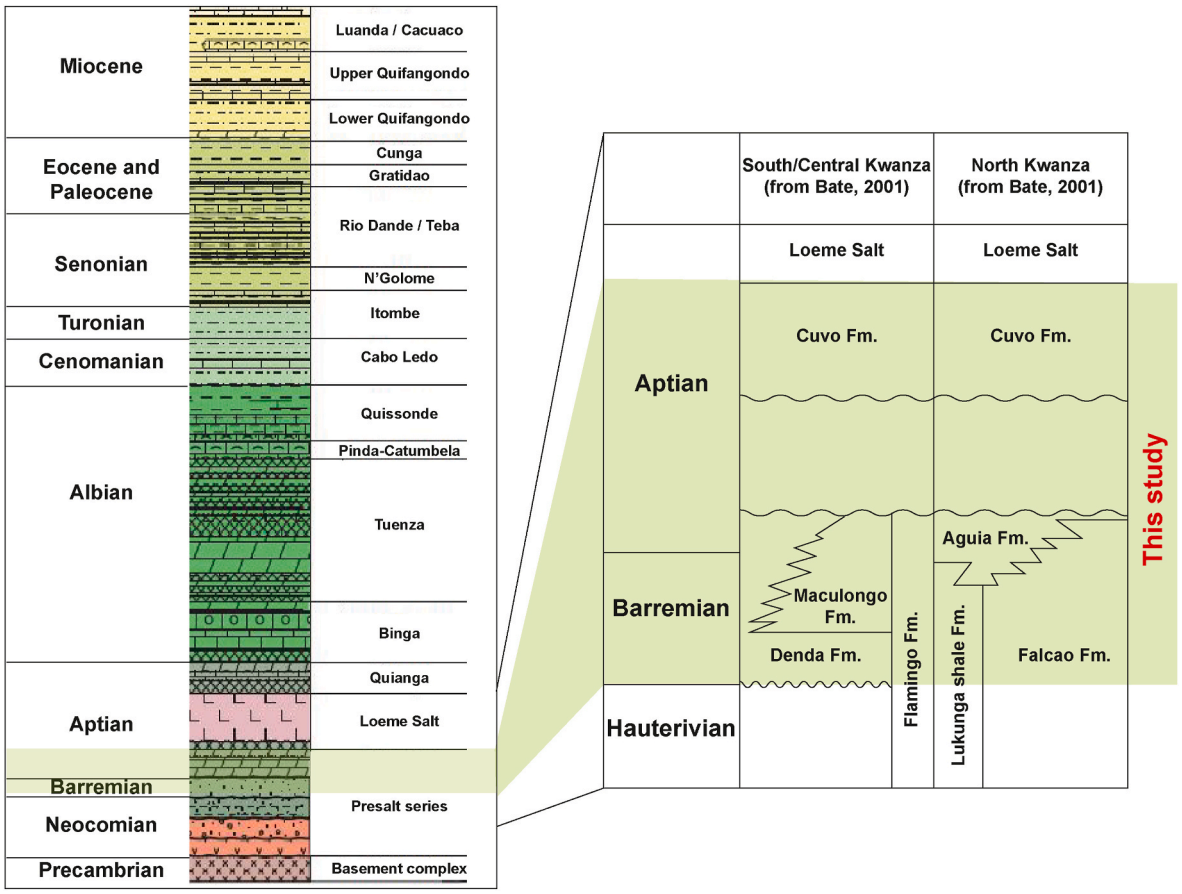

Fig. 3. General stratigraphic log of the offshore Kwanza basin with details on the Barremian-Aptian interval (adapted from Brownfield and Charpentier, 2006; Bate et al., 2001).

paleoenvironmental zones, namely North Kwanza and South/Central Kwanza. In the North Kwanza area, sedimentary sequences include Valanginian to Barremian deep-water shales (Lukunga sandstone Fm), Barremian/Aptian deltaic sands (Aguia Fm), and Neocomian to Aptian carbonate shelf deposits within sag-basin lakes (Falcao Fm). The South/Central Kwanza area encompasses the Barremian to lower Aptian Denda Fm (conglomeratic fan), partly contemporaneous with siliciclastic, shale, and salt deposits of the Muculungo Fm. The volcanic deposits of the Kwanza basin are consolidated under the Flamingo Fm, described by Bate et al. (2001) as an undifferentiated term encompassing all contemporaneous volcanism occurring during clastic and carbonate deposition. This formation comprises lava flows, basalts, and green volcanic ash deposited in lacustrine environments.

Both areas are overlain by a significant unconformity, corresponding to the hyper extension stage between Africa and South America. The Cuvo Fm comprises litharenite/conglomerates grading upwards to claystones, carbonates, and evaporites (Bate et al., 2001). The Loeme Fm, dating back to the Aptian period, marks the onset of marine transgression with a carbonate sequence formed in a marine-lagoonal setting. Succeeding this, the late Aptian to Albian period witnessed a shift to transitional carbonate-evaporite cycles, as seen in the Quianga, Binga, and Tuenza formations. The subsequent period from the Albian to the Senonian (Coniacian to Maastrichtian) was characterized by the extensive spread of organic-rich marine mudstones and marls, as exemplified by the lithological succession from the Quissonde to Rio Dande/Teba formations, which developed both laterally and atop the carbonate structures (e.g. Pinda-Catumbela Fm and basal Quissonde Fm). The Paleogene to Neogene stratigraphy is characterized by an initial retrogradation in marine environments. The sequence, from the base upwards, includes: 1) The Rio Dande Fm from the Paleocene, known for its detrital limestones and sandstones. 2) The Gratidão and Cunga formations from the Eocene, comprising regressive sandstones and siltstones, turbidites, and deep-marine deposits. 3) The Quifangondo Fm from the Miocene, distinguished by prograding clastic sediments (channel-filled sandstones and turbidites). 4) The Luanda Fm, spanning from the late Miocene to the Pliocene and Pleistocene, recognized for its deltaic-continental terrigenous clastic sequence.

2.3. *Structural evolution of the Outer Kwanza basin*

The Outer Kwanza basin initially formed during the early Cretaceous rifting associated with the opening of the South Atlantic ocean. Rifting was recorded by the development of horst-and-graben systems in the present offshore area (Brownfield and Charpentier, 2006; Guiraud et al., 2010; Hudec and Jackson, 2002, 2004; Karner and Driscoll, 1999). The structural map of the top of the pre-salt carbonates in the investigated domain shows two main strikes of deep, presumably basement rooted normal faults, N-S and NW-SE (Erdi and Jackson, 2021, Fig. 4A). Few faults with a NE-SW strike are also observed. This fault pattern is consistent with the regional structural pattern previously described for the Angolan margin (Moulin et al., 2005), and is very similar to the normal fault pattern observed at the top of the TOCA Fm in the Lower Congo basin (Bah et al., 2023a).

The late syn-rift to post-rift Aptian salt controlled the post-rift, gravity-driven deformation and the overall tectono-stratigraphic evolution of post-Aptian sequences in the Outer Kwanza basin since the Albian (Duval et al., 1992; Lundin, 1992; Quirk et al., 2012; Erdi and Jackson, 2021). This gravity-driven salt-tectonic system consists of kinematically-linked zones of updip extension above the Flamingo platform and downdip contraction towards the seaward edge of the salt

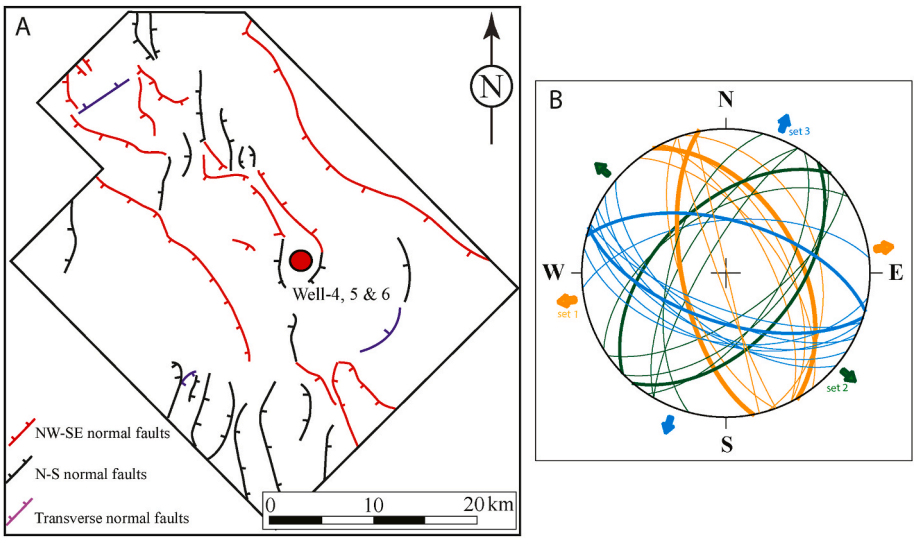

Fig. 4. A. Schematic map of the normal fault pattern at the top of the carbonate pre-salt sequences (after Erdi and Jackson, 2021). B. Stereodiagram (equal area, lower hemisphere) showing the mesoscale normal faults and extension fractures measured in the cores. Colors correspond to sets defined according to consistent geometry and kinematics, with inferred related direction of extension. 1, 2 and 3 refer to relative chronology between sets inferred from few observations on cores.

(Hudec and Jackson, 2002, 2004) accompanied with significant rotation of the overburden (Erdi and Jackson, 2021). Post-rift thermal subsidence caused regional seaward tilting of the margin during the Cenomanian onwards, causing seaward gliding, translation and to some extent rotation of the detached overburden at various rates above the base-salt relief.

3. Materials and methods

3.1. Studied material

The studied material consists of cores of the deeply buried pre-salt carbonates of the Outer Kwanza basin (Fig. 2). These carbonates were drilled at an approximate depth interval of 4500–5000 m (precise depths not provided for confidentiality reasons) by three nearby ultra deep wells located in the Outer Kwanza basin (Figs. 2 and 4A). For this study, we focused on a dolomitized microbialite limestone facies recognized in the three wells and corresponding to core portions of 13 m long in Well-4, 13 m long in Well-5 and 20 m long in Well-6 (Fig. 5). The studied pre-salt carbonates are slightly deeper from Well-4 to Well-6 within the 4500–5000 depth interval (Fig. 5). The investigated core portions show bedding-parallel sedimentary stylolites and few tectonic stylolites as well as mesoscale fractures and faults (Fig. 6).

3.2. Methods

3.2.1. Optical and cathodoluminescence microscopy

Petrographic observations of 30 thin-section were conducted under natural light and cross polars using a Zeiss Axioplot polarizing microscope equipped with a Nikon Digital DS_U2/Ds_Fi1 camera. The diagenetic phases were characterized using a NewTec scientific Cathodyne model CATHOD-SP01 equipped with an IDS UI-3850CP-C-GL R camera, under conditions of vacuum of 90 mTorr, 12–15 kV voltage and 200 μA intensity for the electron beam. All analyses were done at TotalEnergies Centre Scientifique et Technique Jean Féger (CSTJF), Pau, France.

3.2.2. U -Pb dating of carbonate material

U–Pb dating of carbonates was carried out at Centre Européen de Recherche et d'Enseignement des Géosciences de l'Environnement (CEREGE), Aix-en-Provence, France) by Laser Ablation- High Resolution Inductively Coupled Plasma Mass Spectrometry (LA HR-ICP-MS) following the methodology described in Godeau et al. (2018) and in Bah et al. (2023b). The equipment consists of an ArF 193 nm, 4 ns excimer laser (ESI, Elemental Scientific Industries) and an HR-ICP-MS with magnetic sector (Element XR, Thermo fisher). Analyses were conducted on five thick (~100 μm) polished sections exhibiting areas of carbonates of interest. The samples were first scanned (3200 dpi resolution) to facilitate the navigation when placed in the sample cell. An initial screening phase was first conducted to investigate U and Pb concentrations and U/Pb ratio variation over the entire thick section in order to select the best areas for the final measurements (Roberts et al., 2020). Analyses were done with a laser spot size of 150 μm. The ablation speed is of the order of 1–1.5 μm/s under standard conditions, it is preceded by a pre-ablation phase of a few seconds to clean the sample surface. Samples were measured by a standard bracketing approach, using the NIST-614 glass standard for instrumental drift and lead isotope composition (Woodhead and Hergt, 2001) and the WC-1 natural calcite standard for inter-elemental fractionation (reference age = 254.4 ± 6.4 Ma; Roberts et al., 2017). A total of 24–48 ablation spots were performed for each microsite analyzed. Detailed spot-by-spot assessment was carried out afterwards by examining ablation pits under CL microscopy. The U–Pb isochrone ages were calculated in a Tera-Wasserburg diagram using the Isotplot 4.15 add-on (Excel).

3.2.3. Inversion of sedimentary stylolite roughness for burial stress

Bedding-parallel (sedimentary) stylolites (BPS, hereinafter) are common serrated mesostructures that form in response burial-related pressure solution under a vertical maximum principal stress σ1 parallel to the peaks of the stylolites (e.g., Koehn et al., 2007). The analysis of the signal carried by their roughness (i.e., the difference in height between two consecutive points separated by a set length of observation) can be used to constrain the maximum depth of active compaction-related pressure-solution in carbonate rocks (Schmittbuhl et al., 2004; Ebner et al., 2009b; Rolland et al., 2014; Koehn et al., 2012, 2022; Bertotti et al., 2017; Beaudoin et al., 2019; Bah et al., 2023b; Zeboudj et al., 2023), regardless of the past geothermal gradient and fluid pressure (Beaudoin and Lacombe, 2018).

The inversion process relies on the self-affine properties of the stylolite final roughness, acquired quasi instantaneously with regard to the geological time scale (~200 years, Aharonov and Katsman, 2009). The spatial transform of the signal defined by the roughness of a stylolite along its track can be defined by two self-affine scaling regimes, hence by two different Hurst exponents (Schmittbuhl et al., 2004): the Hurst exponent equals 0.5 at the large scale (typically >1 mm), a value typical

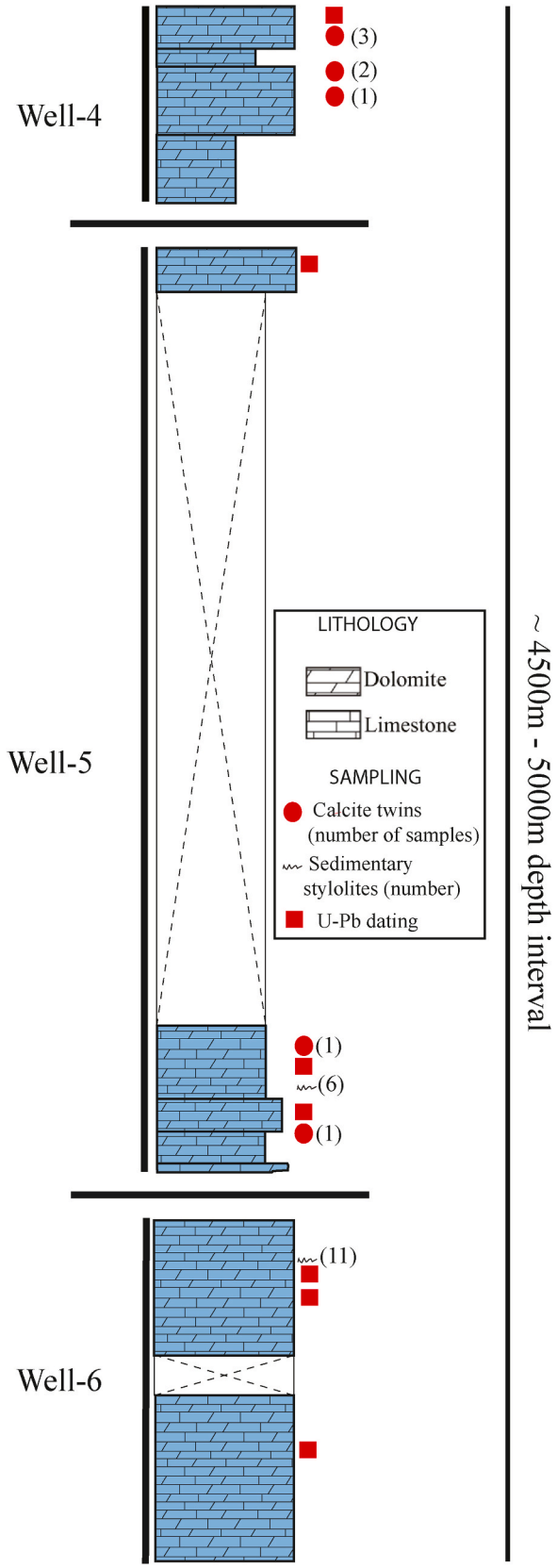

Fig. 5. Schematic representation of the studied cores within the studied pre-salt carbonates. The cores have been arbitrarily placed on top of each other, in an attempt at reflecting that the intervals of interest were drilled at greater depth from Well-4 to Well-6. For confidentiality reasons, the entire cores are not depicted and the exact depths of coring within the 4500–5000m depth interval are not reported.

of the elastic energy, while it equals 1.1 at a smaller scale (typically <1 mm), suggesting an effect of the surface energy (Schmittbuhl et al., 2004).The spatial scale at which there is a transition between these two regimes, the so-called crossover length Lc is directly related to the magnitude of the prevalent mean and differential stresses in the strata at the time the stylolite stopped to be an active dissolution surface.

For their analysis, stylolites are cut along two orthogonal faces, both perpendicular to the stylolite plane and parallel to the peaks. Each face is then polished and scanned in 2-D with a 12,800 dpi resolution, the 2-D track is digitized, then its average trend is set horizontally and to a value of 0. A nonlinear regression with two set slopes corresponding to the Hurst exponents (0.5 and 1.1) is used with regularly binned FPS data to find the Lc value, with an intrinsic uncertainty of ~23% (Rolland et al., 2014).

For sedimentary stylolites, the magnitude of the in-plane stress is expected to be isotropic ($\sigma H = \sigma h = \sigma 2 = \sigma 3$) and smaller than the magnitude of the vertical stress $\sigma_v = \sigma 1$:

$$\sigma_H = \sigma_h = \left(\frac{\nu}{1-\nu}\right)\sigma_v \quad \text{(Eq 1)}$$

where ν is the Poisson ratio, so the relationship between the cross-over length (noted Lc in m) and vertical stress magnitudes can be simply expressed as (Ebner et al., 2009b):

$$\sigma_v^2 = \frac{\gamma E}{\alpha L_C} \text{ with } \alpha = \frac{(1-2\nu)(1+\nu)^2}{30\pi(1-\nu)^2} \quad \text{(Eq 2)}$$

where γ is the surface energy at the solid-fluid interface and E is the Young modulus.

The validity of the hypothesis of stress isotropy in the plane of the stylolite this equation relies upon is tested by comparing the Lc obtained from the 2 oblique cuts, which should be similar within methodological uncertainty.

The maximum depth at which the stylolite stopped being active is obtained by the equation: $\sigma_V = \rho g h$ with ρ the density of the rock column above the stylolite ($kg.m^{-3}$), g the gravitational field acceleration ($m.s^{-2}$), and h the depth at which the dissolution along the stylolite halted (m). Noticeably, the chemo-mechanical model assumed for the Stylolite Roughness Inversion Technique (SRIT) considers that the dissolution occurs on a pressurized plane at the fluid-rock interface (Toussaint et al., 2018); therefore, the conversion of σ_v into depth is independent on the surrounding fluid pressure, so the value of ρ used in the calculation corresponds to the dry density of the rock column for (Ebner et al., 2009b).

The uncertainty on γ is negligible (Wright et al., 2001) and the one for α is very low considering the limited range of variations of the Poisson ratio in carbonates (Ji et al., 2018). Because it weighs more than the other parameters in equation (2), the value of E requires calibration by mechanical tests. Then, the 23% uncertainty on the value of Lc is the main source of uncertainty in the calculation of σ_V. Following equation (2) that links σ_V to the square root of Lc, the final uncertainty on the magnitude of σ_V amounts to 12% (Rolland et al., 2014).

When applied to a population of BPS, SRIT yields the range of depths in which compaction-induced pressure solution was active under a vertical maximum principal stress σ1 (e.g. Beaudoin et al., 2019; Labeur et al., 2021, 2024; Bah et al., 2023a,b; Zeboudj et al., 2023). The combination of this paleopiezometric approach with burial modeling further reveals the time at which the burial-related vertical stress stopped being the maximum principal stress σ1 (Beaudoin et al., 2020a). Assuming that the prime reason for a population of BPS to stop their development is that the burial-related stress becomes lower than the horizontal tectonic-related stress, i.e., σ1 switches form vertical to horizontal, the absolute age of the onset of horizontal shortening can be inferred. This approach has been validated in tectonized sedimentary basins (Beaudoin et al., 2020a,b) and in fold-and-thrust belts (Labeur et al., 2021, 2024; Lacombe et al., 2021), even though alternate reasons for the halt

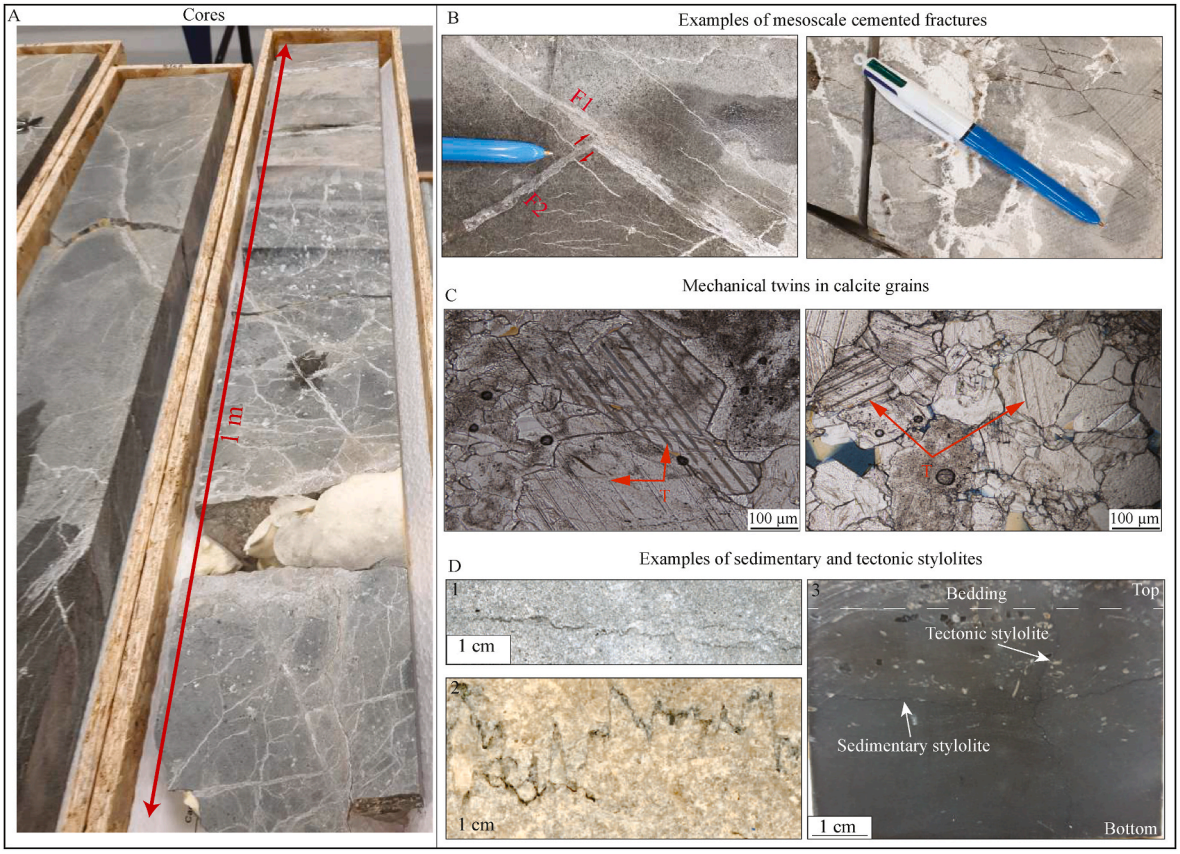

Fig. 6. General (A) and detailed (B, C and D) photographs of a studied core and the mesoscale-microscales structures observed/sampled for analyses. T denotes twins.

of pressure solution at depth may be diverse, e.g., a saturation effect at the stylolite plane scale related to the depth of deformation (Toussaint et al., 2018); clogging of the porosity due to dissolved material reprecipitation that prevents further development of the stylolite plane (Hou et al., 2023); local fluid overpressure effect (Bah et al., 2023b).

3.2.4. *Construction of a burial-time model*

In order to reconstruct the burial evolution of pre-salt carbonates over time, we have built a 1-D burial-time model for Well-4 using TemisFlow™ basin modelling software. The workflow, already described in Bah et al. (2023b) is summarized below.

The burial-time simulation consists in the backstripping (backward modeling) of the stratigraphic column followed by a forward simulation of the sequence of deposition and erosion of the full section. Available seismic interpretations (TotalEnergies internal maps) were used to define the erosional or non deposition phases. The backstripping process allows for the inversion of the evolution of the basin geometry (Perrier and Quiblier, 1974). For each period defined in the chronostratigraphic

Table 1
Parameters used in burial modelling.

Event		Age (Ma)		Today thickness	Initial thickness	Model lithology	Initial porosity	Solid density	Top (computed)
Formation	Age	From	To	m	m		%	kg/m^3	TVDSS (m)
Quifangondo-Luanda	Miocene	23	0	967	1057	90% sandstone, 10% shale	48	2670	1677
Cunga	Priabonian	41	34	271	400	90% shale, 10% siltstone	63	2650	2734
Gratidao	Eocene	56	41	138	285	80% limestone, 20% shale	53	2700	2915
Rio Dante	Paleocene	66	56	81	120	50% marl, 40% lmst, 10% sst	53	2690	3053
lto mbe-N'Golome	Upper Cretaceous	94	66	557	775	60% marl, 40% limestone	54	2690	3134
Cabo Ledo	Cenomanian	100	94	99	185	80% shale, 20% marl	65	2650	3691
Quissonde	Upper Albian	103	100	194	315	60% marl, 40% limestone	54	2690	3790
Tuenza	Middle Albian	105	103	65	80	50% limestone 50% dolostone	50	2790	3984
Binga	Lower Albian	113	105	149	245	50% limestone, 50% anhydrite	50	2870	4049
Loeme	Aptian Salt	118	113	118	125	80% halite, 20% anhydrite	10	2350	4198
Upper Cuvo	Lower Aptian	125	118	32	40	100% 1imestone	38	2710	4316
Flamingo	Barremian	130	125	348	380	80% sst, 20% limestone	48	2670	4348 4696

column, after removing the top layer, the remaining sedimentary formations are decompacted (or compacted in the case of erosion), by using porosity vs depth or compaction curves (Atashbari and Tingay, 2012). Additional physical properties such as thermal conductivity, heat capacity and radiogenic production, as well as the constitutive law for compaction were defined with respect to the ratio of the different sedimentary rocks (limestone, shale, sandstone) described in the layer. The formation properties are reported in Table 1. The restoration was performed from the present day to the deposition of the earliest syn-rift TOCA eq first layer at 130 Ma. The results of the backstripping is the evolution of thickness with time for each layer.

From the reconstruction of the depth-time evolution of each strata the evolution of the porosity is modelled. This forward simulation of the 1-D sections is performed considering a hydrostatic pressure regime, no hydrocarbon production and a porosity vs depth law (e.g. Atashbari and Tingay, 2012). The calibrated porosity vs depth empirical law used in the simulation represents porosity evolution that is controlled by both mechanical compaction (grain framework tightening) and chemical compaction (dissolution along grain-to-grain contacts).

3.2.5. *Inversion of calcite twins for tectonic stress*

Mechanical twinning has been for long recognized as a common mechanism of low pressure/low temperature plastic deformation of calcite (Burkhard, 1993; Lacombe et al., 2021). Twinning occurs by an approximation to simple shear in a specific direction and sense along the e crystallographic planes. Twinning activation is negligibly affected by strain rate, temperature and confining pressure, and depends mainly on differential stress, grain size and strain (Turner, 1953; Turner et al., 1954; Rowe and Rutter, 1990; Laurent et al., 2000; Lacombe et al., 2021).

The inversion of calcite twins for stress is a well established technique (see review in Lacombe, 2007, 2010; Lacombe et al., 2021) that enabled the reconstruction of paleostress orientations and magnitudes in a variety of settings, including sedimentary basins (Lacombe et al., 1990, 1994; Lacombe and Laurent, 1996; Kulikowski and Amrouch, 2017; Zeboudj et al., 2023; Bah et al., 2023b), fold-and-thrust belts (Craddock et al., 1993, 2016, 2018; Lacombe et al., 2021; 1996, 2007, 2009; Harris and van der Pluijm, 1998; Amrouch et al., 2010, 2011; Rocher et al., 1996; Beaudoin et al., 2016; Arboit et al., 2015; Lacombe, 2001) and even at passive margins (Bah et al., 2023a; Zeboudj et al., 2023) and oceanic domains (Craddock et al., 1993; 2004; Brandstätter et al., 2017). Calcite twin analysis requires only limited rock volumes and is therefore an efficient tool to reconstruct the paleostress history from well cores (e.g., Lacombe et al., 1994; Rocher et al., 2000; Bah et al., 2023a; Zeboudj et al., 2023). In this study, the investigated cores were oriented a posteriori by comparison with the FMS (Formation Micro-Scanner) images of the well. The distribution of the samples in the investigated cores of the 3 wells is shown in Fig. 5. For each sample, calcite twin data were collected from three mutually perpendicular thin-sections oriented with respect to the generator of the cores following the procedure described in Bah et al. (2023a). In each thin section, the orientations of twin lamellae and of optical axes were measured from 20 to 30 grains using a Universal Stage.

Basic conditions for valid inversion of calcite twin data for stress involve (1) low twinning strain which can be approximated by coaxial conditions so the orientation of twinning strain is reliably correlated with paleostress orientation (Burkhard, 1993; Amrouch et al., 2010; Wakamori and Yamaji, 2020) and (2) homogeneous stress field at the scale of the grain/aggregate. Twinning occurs if the applied resolved shear stress τ_s is equal to, or greater than, the Critical Resolved Shear Stress (CRSS) for twinning τ_a (Jamison and Spang, 1976; Tullis, 1980; Lacombe and Laurent, 1996; Ferrill, 1998; Laurent et al., 2000). The meaning and the value of the CRSS to be used during the inversion process have been recently discussed by Lacombe et al. (2021). Thus, one assumes that for twinned planes: $\boldsymbol{\tau}_s \geq \boldsymbol{\tau}_a$ and for untwinned planes: $\boldsymbol{\tau}_s < \boldsymbol{\tau}_a$. Since the CRSS is grain-size dependent (its value being smaller for large grains than for small grains for which twinning is more difficult), we first determined the dominant 2-D grain size in sample by adding the length of the long and short axes of the grain and dividing the sum by 2, then we discarded the under-represented smallest and/or largest sizes. The CRSS being also dependent on strain since calcite hardens once twinned (Lacombe et al., 2021), we roughly estimated twinning strain by dividing the cumulative thickness of all twin lamellae of a given set in a grain by the length of the grain measured perpendicular to the twins. Knowing these two parameters, the appropriate CRSS value τ_a to be used for the quantification of differential stress magnitudes was selected using the empirical curves published by Parlangeau et al. (2019). As in Bah et al. (2023a), the retained value was checked for consistency against the estimated temperature of deformation at each stage of the burial history.

The Calcite Stress Inversion Technique (CSIT-2) used in this study allows the recognition and separation of successive paleostress tensors from sets of calcite twins (Parlangeau et al., 2018). The principle of the inversion is to identify the stress tensors which verify the inequalities (1) for the largest number of twinned planes and the whole set of untwinned planes. The solution is searched as a reduced stress tensor with 4 parameters: the orientations of principal stress axes (σ_1, σ_2, σ_3) and the stress ratio (Φ):

$$1 \geq \Phi = \frac{\sigma 2 - \sigma 3}{\sigma 1 - \sigma 3} \geq 0 \text{ with } \sigma_1 \geq \sigma_2 \geq \sigma_3 \quad \text{(Eq 3)}$$

Considering the complete dataset (twinned and untwinned planes), the first step of the process consists of a systematic search in the 3-D space for the three Euler angles (which define the orientations of the principal stress axes) with a regular interval of 10°, the stress ratio being fixed at 0.5, in order to select the reduced stress tensors accounting for at least 20% of twinned planes. For each tensor, the penalization function f defined as:

$$f = \sum_{j=1}^{j=n} \left(\tau_s^j - \tau_s^{min}\right) \quad \text{(Eq 4)}$$

with τ_s^j the resolved shear stress applied on the j untwinned planes such as $\tau_s^j \geq \tau_s^{min}$ and τ_s^{min} the smallest resolved shear stress applied on the twinned planes compatible with the tensor, is calculated. The function f should equal 0 for a perfect dataset and its value increases with the incorporation of incompatible untwinned planes into the solution. The stress tensors with a function $f < 0.5$ are selected and each of them is weighted by the number of its nearest neighbours according to a similarity criterion. This enables the automatic identification of different groups of tensors that are associated with a high percentage of compatible twinned planes and low values of the function f. The reference reduced stress tensor of each cluster is then applied to all twinned and untwinned planes, while the percentages of twinned planes to be explained are progressively increased. The optimal tensor is obtained when 1) the maximum number of twinned planes are taken into account; 2) the minimum number of untwinned planes are taken into account; 3) the value of the function f is minimal. More details can be found in Parlangeau et al. (2018) and Lacombe et al. (2021).

For each stress tensor, the inversion yields the orientation of the principal stress axes (σ_1, σ_2, σ_3), the stress ratio (Φ) and a non-dimensional differential stress $\frac{(\sigma_1 - \sigma_3)}{\tau a}$ which is related to the final value of τs^{min}:

$$\frac{(\sigma_1 - \sigma_3)}{\tau a} = \frac{1}{\tau s^{min}} \quad \text{(Eq 5)}$$

Knowing the value of τa for each sample, we then determine for each state of stress the values of the differential stresses (σ_1-σ_3) and (σ_2-σ_3) using equations (3) and (5). The methodological uncertainty associated with the stress results is ±10° for the orientations of the principal stresses, ±0.1 for the stress ratio and ±30% for the values of the

differential stresses as derived from the application of CSIT-2 on numerically generated twin datasets (Parlangeau et al., 2018).

3.2.6. Fracture analysis

Fracture orientation data were collected from the cored intervals. Fractures of various types were directly measured on the core (Fig. 4B) using a compass equipped with a clinometer, positioning the generator to the North, then correcting from the real orientation of the generator. When possible, the deformation mode of fractures (opening or shearing) was determined. Depending on their orientation and deformation mode, the geometry and the kinematics of the fracture sets were related to the activity of the regional faults and/or to the stress regimes reconstructed from calcite twins.

4. Results

4.1. Macroscopic and microscopic petrographic evolution

On the basis of observations on cores and thin sections, a single bioclastic sedimentary facies has been identified in all of the three studied cores. This facies consists mainly of packstone to boundstone microbialite in individual beds ranging in thickness from a few cm to 20 cm, with blurred and generally gradual microbial bed boundaries (Fig. 7). At core scale, the microbial beds show limited macroscopic intervals of diagenetic alteration (of silica, dolomite and calcite). However, at the thin-section scale, the diagenetic sequence appears to be the same throughout the cored interval.

The detailed description of the complete diagenetic evolution of the studied presalt carbonates is not the subject of this study, so we present only the main diagenetic events recognized in the cores. These events follow deposition of the primary matrix calcite M in the form of spherules or (micro)sparite and include, in chronological order (Fig. 7), very early dolomitization, early silicification, “late” precipitation of blocky calcite C and chemical compaction (development of bedding-parallel stylolites). Blocky Calcite C precipitated as vug and pore filling cement and as late vein filling. Dolomite appears mainly as a replacement of primary matrix calcite (M) and locally as intergranular cement. Silica is present in the form of pore-filling micro-quartz (cement) and primary calcite-replacing silica/calcedony. Silica is most common along fractures where the surrounding matrix is strongly cemented. Thin-section observations show that blocky C calcite postdates dolomite and silica. Pressure-solution affects primary calcite (M), calcite cement C, silica and dolomite and therefore appears to have been active throughout most of the diagenetic history (Fig. 7).

4.2. U-Pb age of dolomite

Only the dolomite phase has yielded reliable U-Pb ages. U-Pb dating was not attempted for primary matrix calcite M and was unsuccessful for the blocky calcite cement C (no U-Pb signal). 8 samples were dated, including 1 sample from Well-4, 4 samples from Well-5 and 3 samples from Well-6 (Fig. 5). Fig. 8 shows examples of Tera-Wasserburg diagrams illustrating the good quality and the consistency of the U-Pb ages obtained in Well-5) (see also Supplementary Material). The age obtained for the Well-4 core dolomite is 119.8 ± 3.4 Ma. Samples from the Well-5 core yielded ages of 118.7 ± 3.0 Ma, 117.1 ± 1.7 Ma, 116.3 ± 3.4 Ma and 107.6 ± 2.5 Ma; and those from the Well-6 core, 114.4 ± 2.3 Ma, 111.3 ± 1.3 Ma and 110.4 ± 1.9 Ma.

The U-Pb ages above indicate that dolomite roughly precipitated in the interval ~125-108 Ma. The dolomite appears to be slightly older from Well-4 (~120 Ma) to Well-5 (~115 Ma) and Well-6 (~112 Ma), being overall mainly of Aptian age. Since the depositional age of the studied presalt carbonates is in the range 130-113 Ma (Barremian-Aptian), dolomite appears to have formed sub-synchronous to deposition or very early in the diagenetic history of the pre-salt carbonates.

4.3. Maximum depth of active pressure solution from stylolite roughness inversion

Six samples containing BPS were cut (Figs. 5 and 6), from which 21 2-D traces were analyzed by the Fourier Power Spectrum (FPS; Fig. 9A) method. Among these 21 BPS traces 17 displayed two self-affine regimes with the expected Hurst coefficients (Table 2). Fig. 9 shows four examples of treatment. The treatments in Fig. 9 B and C are acceptable, as the inversion provides a trend showing two well-marked slopes with Hurst coefficients consistent with those predicted by the growth model. On the other hand, Fig. 9D illustrates a failed case since the inversion process returns a single slope.

The natural variability of the Poisson’s ratio in carbonates is rather low (0.18–0.35, e.g. Ji et al., 2018), and the impact of this uncertainty on the calculation of the stress is only about 10% for extreme values. In contrast, the impact of the Young modulus E, which varies between 5 GPa and 100 GPa (Hadi and Nygaard, 2023) in carbonates namely according to porosity, is more important. It is difficult to evaluate whether the E value determined in the laboratory is suitably representative of the E at the pressure conditions at which deformation occurs (e.g. Pimienta et al., 2015). However, Labeur et al. (2024) suggested that sedimentary stylolite roughness inversion for stress should rely upon the value of the Young modulus determined from stress-strain plots from mechanical tests applied to homogeneous, undeformed portions of the studied formation, because this value expectedly returns the highest value of E, hence the closest to the one prevailing at the time the deepest stylolite stopped its development.

In order to calculate the vertical stress value during the pressure-solution activity period along the stylolites, we used the mean values of the elastic parameters determined from geomechanical tests that were run on the pre-salt carbonates from several wells, $E = 25$ GPa and $\nu = 0.27$ (Mastina and Zerbinati, 2021). The uncertainty in the determination of E and ν is ±10% and ±20%, respectively. The stress value was converted into depth considering the dry density of the host rock (2600 kg m^{-3}) and the acceleration of the gravitational field (9.81 m s^{-2}). The value of the resulting vertical stress (σ1) is between 18 and 62 MPa corresponding to a depth range of 750–2500 m (Table 2).

4.4. Burial-time history

The burial model developed for Well- 4 and presented in Fig. 10 shows five phases of burial evolution over time: (1) 130 Ma to 112 Ma, a syn-rift phase with a high mean burial rate of ~40 m/Ma), (2) 112 to 65 Ma, a first post-rift phase with a mean burial rate of ~25 m/Ma, (3) 65 Ma to ~40 Ma, a second post-rift phase of low mean burial rate of ~10 m/Ma, (4) ~40 to ~23 Ma, a third post-rift phase with a short increase followed by a nearly null burial rate and (5) ~23 Ma to present, a fourth post-rift phase of mean burial rate of ~30 m/Ma. Note that the short increase at the late Eocene time (phase 4) was not recognized in the other offshore studies located further north (Bah et al., 2023a; Zeboudj et al., 2023) and might be interpreted as an effect of local thickening of Eocene strata above a halokinetic listric normal fault seen on seismic profiles (internal communication, TotalEnergies). Consequently, the propagation of this thickening to all the sedimentary on the whole column (especially down to the pre-salt sequences) at that time on Fig. 10 is likely to be a numerical artefact that can be neglected. Fig. 10 also shows the distribution of maximum depths of active pressure-solution along sedimentary stylolites as revealed by stylolite roughness inversion.

4.5. Tectonic stresses from calcite twins

Calcite twin inversion was carried out on 8 samples collected in the cores of Well-4 and 5 (Fig. 5). Measurements were carried out in sparite crystals of pristine primary calcispherules, which were not later altered or dolomitized as confirmed by cathodoluminescence observations. The calcite grains all show thin, rectilinear twins Type I twins (Burkhard,

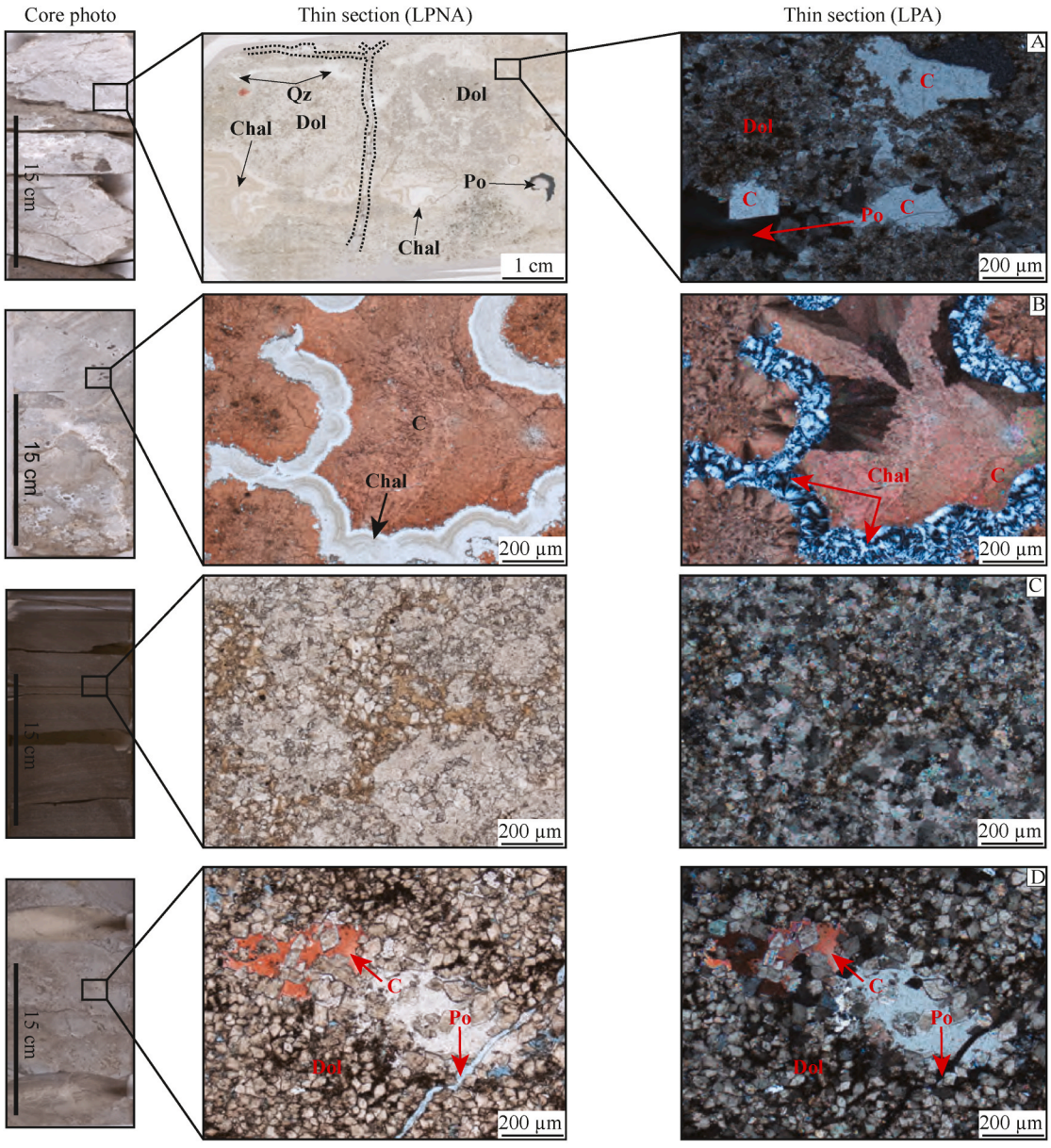

Simplified diagenetic sequence (major events) observed in the cores

Diagenetic event	Paragenetic sequence: Oldest → Youngest
Deposition	
Early calcite M (primary)	
Early dolomitization (replacive)	
Early silicification (replacive and pore filling)	
Blocky calcite C (vug and vein filling)	
Stylolitization	

Fig. 7. Examples of diagenetic processes observed in thin sections under natural light (LPNA) and crossed polars light (LPA). The thin sections were stained with alizarin red S. Calcite appears in red, porosity in blue. (A) Blocky calcite postdating dolomite (Dol). (B) Chalcedony replacing primary calcite. (C and D) Highly silicified and dolomitized petro-facies. Silica and dolomite replace primary calcite. (E) Simplified paragenetic sequence reconstructed from observations on thin sections from cores.

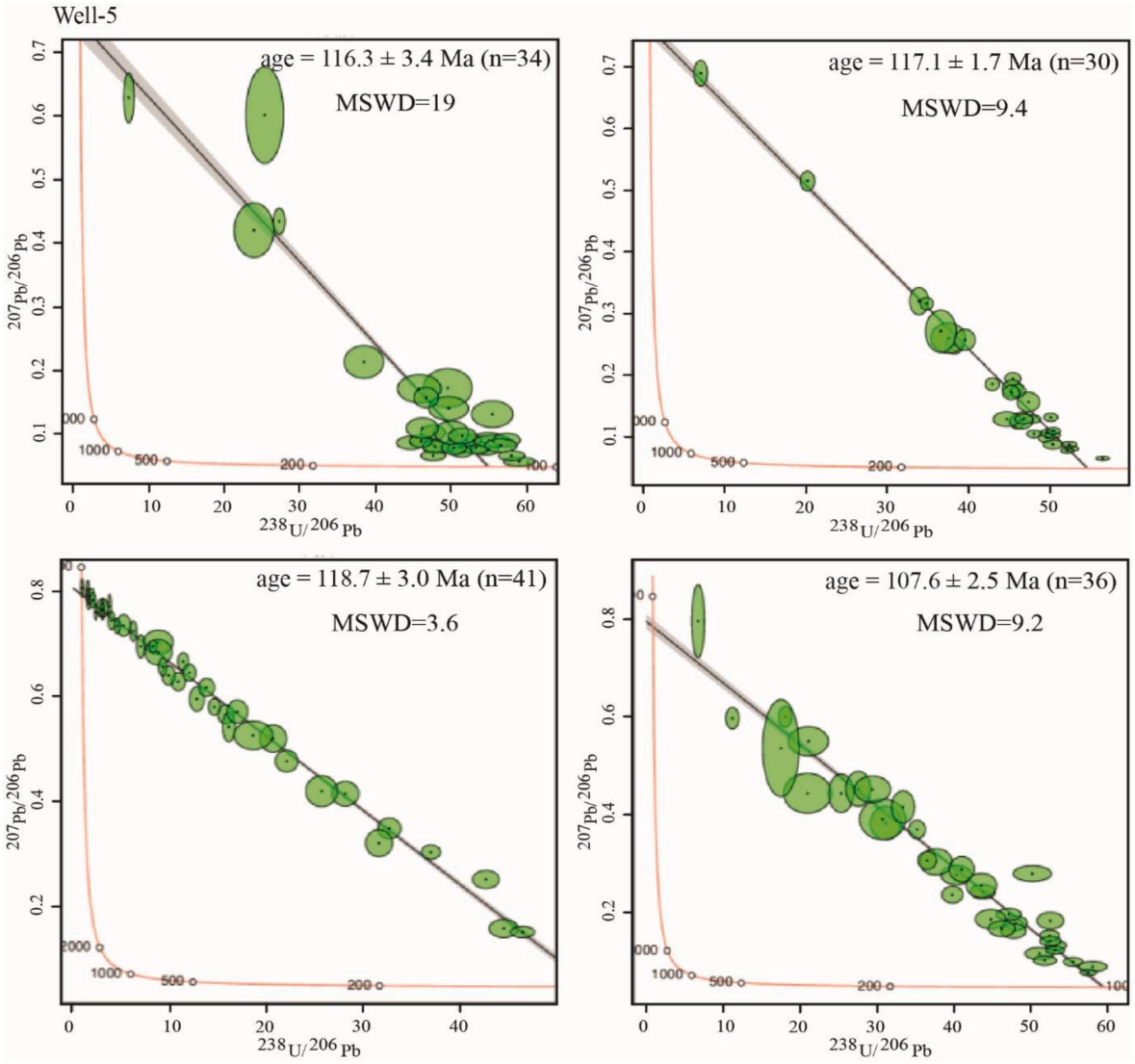

Fig. 8. Examples of Tera–Wasserburg concordia plots for dolomite samples from Well-5 showing 238U/206 Pb vs. 207Pb/206 Pb (n – no. of spots). MSWD – mean square of weighted deviates.

1993)(Fig. 6), indicating deformation at temperatures below 170 °C (Ferrill et al., 2004; Lacombe et al., 2021), in agreement with bottom hole temperatures of about 80–90 °C for the studied wells (unpublished data, TotalEnergies).

We also checked that the distribution of optical axes of grains in our samples was random, which is a prerequisite for the application of the technique (Lacombe et al., 2021). In our samples, the grain size ranges between 50 and 250 μm, with a modal value around 200 μm. Estimated twinning strain remains very low (<2%), which warrants coaxiality between stress and strain. The appropriate CRSS values to be used for the calculation of the differential stress was then defined according to the strain value and the mean grain size of the samples (Lacombe et al., 2021).

Only 2 of the 8 samples analyzed yielded a single stress tensor (Table 3). All other samples (~75%) yielded two or three superimposed stress tensors. To simplify the description of the results as much as possible, the stress tensors obtained were separated into different groups on the basis of consistent principal stress orientations and stress regime (extension, vertical σ1; compression, vertical σ3; strike-slip, vertical σ2). From the 17 types of stress tensors determined from the 8 samples (Table 3), 8 main tensor groups could be defined (Fig. 11): 3 groups of extensional tensors (A, B and C), three groups of compressional tensors (D, E and F), and two groups of strike-slip stress tensors (G and H). The detailed results (principal stress orientations, stress ratios and differential stress magnitudes) are shown in Fig. 11.

For the extensional stress regimes, group A was identified in 1 sample and is characterized by a σ3 oriented N40 (N040°E) and average differential stress magnitudes of 47 MPa for (σ1 - σ3) and 23 MPa for (σ2 - σ3). Group B was identified in 4 samples, with a σ3 ~E-W and average differential stress magnitudes of 34 MPa for (σ1- σ3) and 15 MPa for (σ2- σ3). Group C was identified in 1 sample, with a σ3 orientation ~ NNW-SSE and average differential stress magnitudes of 48 MPa for (σ1- σ3) and 19 MPa for (σ2- σ3).

For the compressional stress regimes, group D was identified in 2 samples with σ1 oriented ~ N45 and mean differential stress magnitudes of 31 MPa for (σ1- σ3) and 10 MPa for (σ2- σ3). Group E was identified in 3 samples with ~E-W oriented σ1 and mean differential stress magnitudes of 43 MPa for (σ1- σ3) and 12 MPa for (σ2- σ3). Group F was identified in 1 sample with a ~N-S oriented σ1 and average stress differential magnitudes of 40 MPa for (σ1- σ3) and 13 MPa for (σ2- σ3).

For the strike-slip stress regimes, group G was identified in 2 samples with a ~N-S oriented σ1 and average differential stress magnitudes of 52 MPa for (σ1- σ3) and 27 MPa for (σ2- σ3). Group H was identified in 3 samples with a ~E-W oriented σ1 and average differential stress

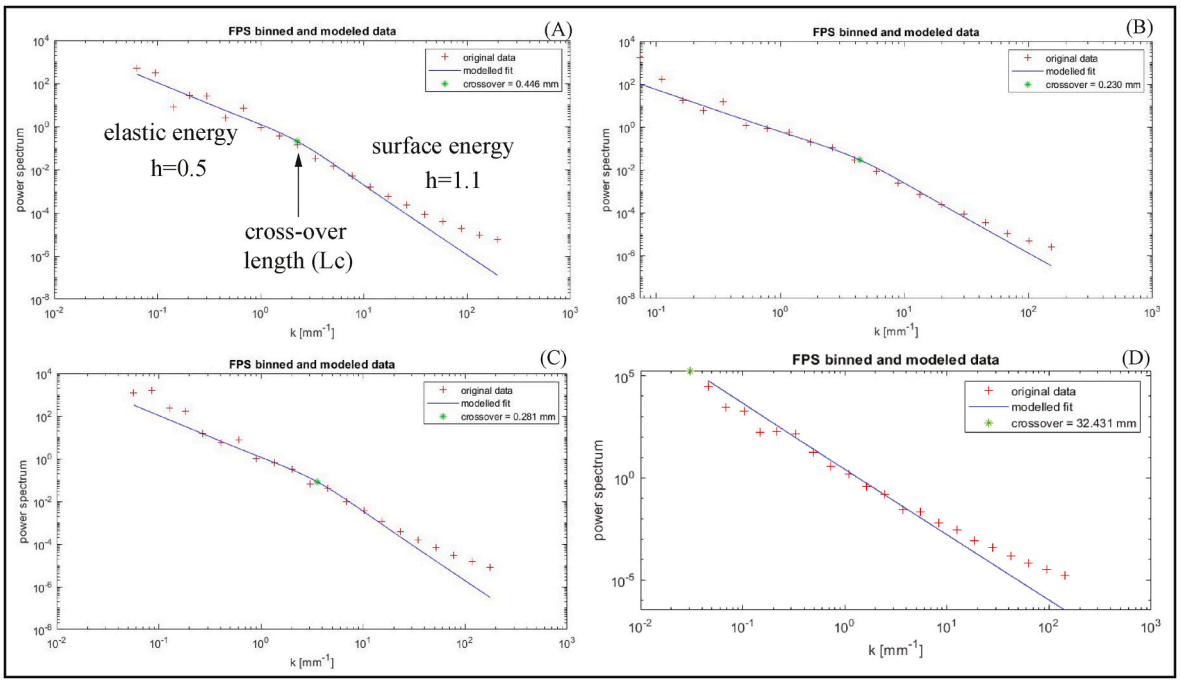

Fig. 9. Spectral analysis of the signal carried by the roughness of sedimentary stylolites. Definition of Hurst exponents and cross-over length on a log-log plot of the Fourier Power Spectrum method (A) and examples of sedimentary stylolite roughness inversion for some samples, either successful (B and C) or failed (D).

Table 2
Results of stylolite roughness inversion applied to sedimentary stylolites in the pre-salt carbonates. σv is calculated with values of E = 25 GPa and $\nu = 0.27$ determined from rock mechanics tests. Uncertainties are 23% on the value of Lc, 12% on the value of the vertical stress (Rolland et al., 2014).

Samples	Cross-over length (mm)	σv (MPa)	Depth (m)
CAM2-1	0.245	48	1950
CAM2-2	0.599	30	1250
CAM2-3	0.446	35	1450
CAM2-4	0.23	49	2000
CAM2-5	0.188	54	2200
CAM2-6	0.489	34	1400
CAM3-1	1.67	18	750
CAM3-2	0.385	38	1550
CAM3-3	0.146	62	2500
CAM3-4	0.281	44	1800
CAM3-5	0.4	37	1500
CAM3-6	0.231	49	2000
CAM3-7	0.251	47	1900
CAM3-8	0.524	33	1300
CAM3-9	0.146	62	1500
CAM3-10	0.922	25	1000
CAM3-11	1.295	21	850

magnitudes of 43 MPa for (σ1- σ3) and 21 MPa for (σ2- σ3).

4.6. Orientation and kinematics of fractures measured in cores

A total of 28 fractures were measured from core samples, most coming from a dolomitic and brecciated interval in the core from Well-6. The fractures are partially to fully cemented. They display various lengths and their dips range between 35° and 90°. Except for the two subvertical mode 1 (extensional) fractures, all other fractures show extensional mixed mode 1-mode 2 kinematics. Despite scattering, the distribution of the fracture directions reveals three main sets (Fig. 4B): a set comprising fractures (10) oriented NNW-SSE (N145° to N165°) and dipping either ~35–60° to the W or to the E (8) or subvertical (2) (set 1 in orange); a set comprising fractures (9) oriented NE-SW (N15° to N45°) and dipping ~50–60° to the NW or to the SE (set 2 in green); and a set comprising fractures (9) oriented (~N85° to N125°) and with variable dips to the N or to the S (set 3 in blue) (Fig. 4B). Chronological relationships (e.g., offsets, abutting) observed on the cores are few and sometimes uncertain, but at first glance they indicate that set 1 seemingly developed first, then set 2, then set 3. Despite the absence of any measured striations, the geometry of most fractures of each set together with their extensional kinematics suggest likely conjugate normal faults roughly consistent with σ3 ~E-W, ~NW-SE and ~NE-SW for set 1, set 2 and set 3, respectively (Fig. 4B).

5. Interpretation of stress results in the Outer Kwanza basin and comparison with the onshore-offshore Congo basin

The results of the inversion of calcite twins document a polyphase paleostress history of the pre-salt sequences of the Outer Kwanza basin. As the calcite M crystals hosting measured twins could not be dated, we constrain its age with the U-Pb age of the replacive early dolomite (~120-108 Ma), which postdates the primary calcite. This pinpoints the precipitation of the studied calcite M at nearly the time of deposition of the carbonate formation, between 130 and ~120-115 Ma (assuming no late diagenetic recrystallisation). The dolomite age can therefore be used to constrain the onset of the reconstructed paleostress evolution (Fig. 10).

The distribution of the maximum depths of activity of BPS as obtained from SRIT projected onto the burial-time curve of the pre-salt carbonates reveals the periods of active compaction-related pressure-solution, hence periods dominated by a state of stress with a vertical σ1. Such a state of stress has prevailed continuously between ~112 and ~57 Ma (750–~2000m) as indicated by 88% (15 over 17) of our stylolite dataset, when including uncertainty but excluding the only two stylolites that recorded active compaction at greater depth (2200 m and 2500 m, Table 2). Considering them would indicate that a vertical σ1 possibly prevailed until either ~38-35 Ma or ~17 Ma, respectively. Although one can wonder about the statistical meaning of the limited dataset supporting active compaction at depth greater than 2000m, one can safely propose that (1) a state of stress with a vertical σ1 prevailed at least between ~112 and ~57 Ma, and (2) that σ1was no longer vertical

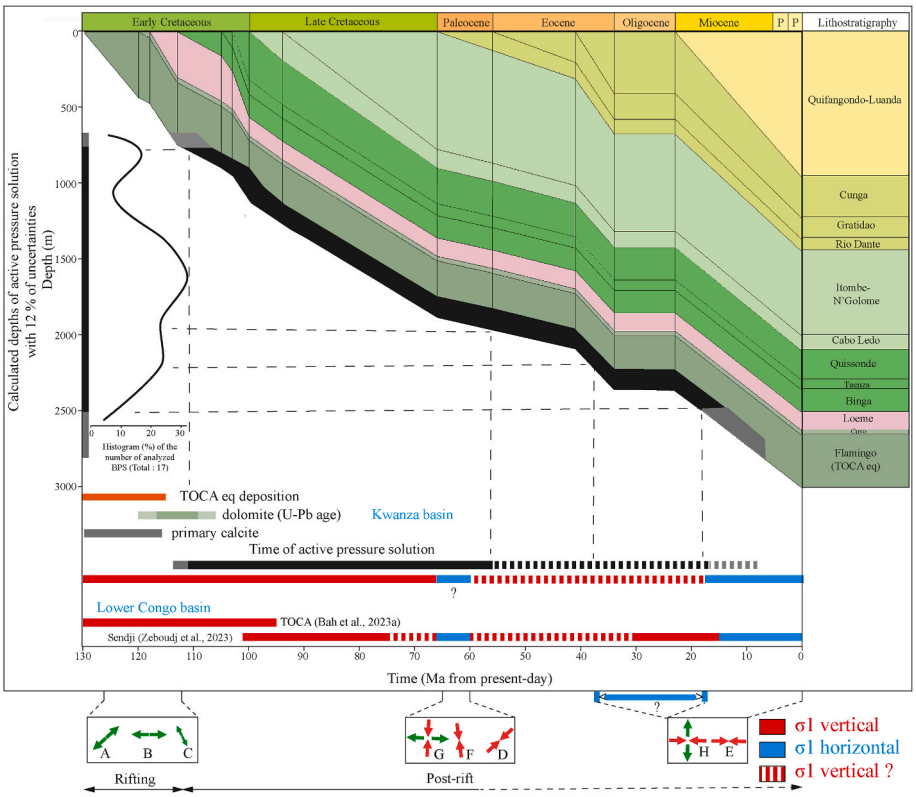

Fig. 10. Burial model constructed from Well-4. The depth on the model is counted from the sea-bed. The calculated depth range of active pressure-solution from bedding-parallel stylolite inversion is reported for the TOCA eq in black on the y-axis, while grey corresponds to uncertainty. The stress regimes revealed by inversion of calcite twins are also reported (map view).

Table 3
Stress tensors determined from inversion of calcite twins. The quality of each tensor is estimated on the basis of several criteria, such as the stability of the principal stress orientations, the value of the penalty function and the number of incompatible untwinned planes.

	σ1 trend (°)	σ1 plunge (°)	σ2 trend (°)	σ2 plunge (°)	σ3 trend (°)	σ3 plunge (°)	Penalization function	Φ	τs^{min}	CRSS MPa	σ1-σ3 MPa	σ2-σ3 MPa	Total number of TP/UP	Number of compatible TP/UP	Quality
Well-4	320	62	204	13	108	24	0.1	0.6	0.175	7	40	24	72/21	20/17	2
	118	21	251	61	20	20	0.1	0.6	0.167		42	25		30/19	1
	6	1	107	83	276	7	0.2	0.3	0.09		78	26		21/18	3
Well-4	338	29	236	20	117	54	0.4	0.4	0.165	7	42	17	124/53	42/44	3
	108	19	225	53	6	30	0.8	0.4	0.116		60	24		52/45	3
Well-4	290	9	23	19	176	69	0.2	0.6	0.187	6	32	20	112/38	35/31	2
	177	50	354	40	85	2	0.2	0.5	0.202		30	14		33/34	1
Well-4	82	15	348	13	220	70	0.4	0	0.099	6	61	0	89/37	37/31	2
Well-4	247	64	56	25	148	4	0.3	0.4	0.145	7	48	19	94/35	37/29	1
	284	68	134	19	40	10	0.4	0.5	0.149		47	23		28/31	2
	239	38	335	7	74	51	0.2	0.2	0.201		35	7		30/28	3
Well-4	257	4	348	20	156	70	0.2	0.4	0.136	6	44	18	176/55	59/49	2
Well-5	22	21	170	66	287	11	0.7	0.9	0.22	7	32	29	141/54	45/46	2
	199	68	333	16	67	15	0.5	0.5	0.213		33	16		42/46	2
Well-5	52	64	183	18	279	18	0.2	0.3	0.245	7	29	9	141/72	42/64	1
	29	6	122	33	290	57	0.4	0.5	0.233		30	15		39/68	1
	74	30	261	60	166	3	0.9	0.4	0.192		36	16		54/29	3

TP/UP: Twinned Planes/Untwinned Planes.
Quality of tensor: decreasing from 1 to 3.

after ~17 Ma (Fig. 10).

Out of the periods during which a vertical σ_1 is likely, either σ_1 has remained vertical (but for instance sedimentary stylolite development decreased or halted in response to reservoir scale fluid overpressure, e.g., hydrocarbon migration in the reservoir or massive cementation/clogging of porosity) or, alternatively, σ_1 has switched to horizontal as a result of the horizontal tectonic stress becoming large enough to overcome the vertical stress. As a result, the timespans without positive

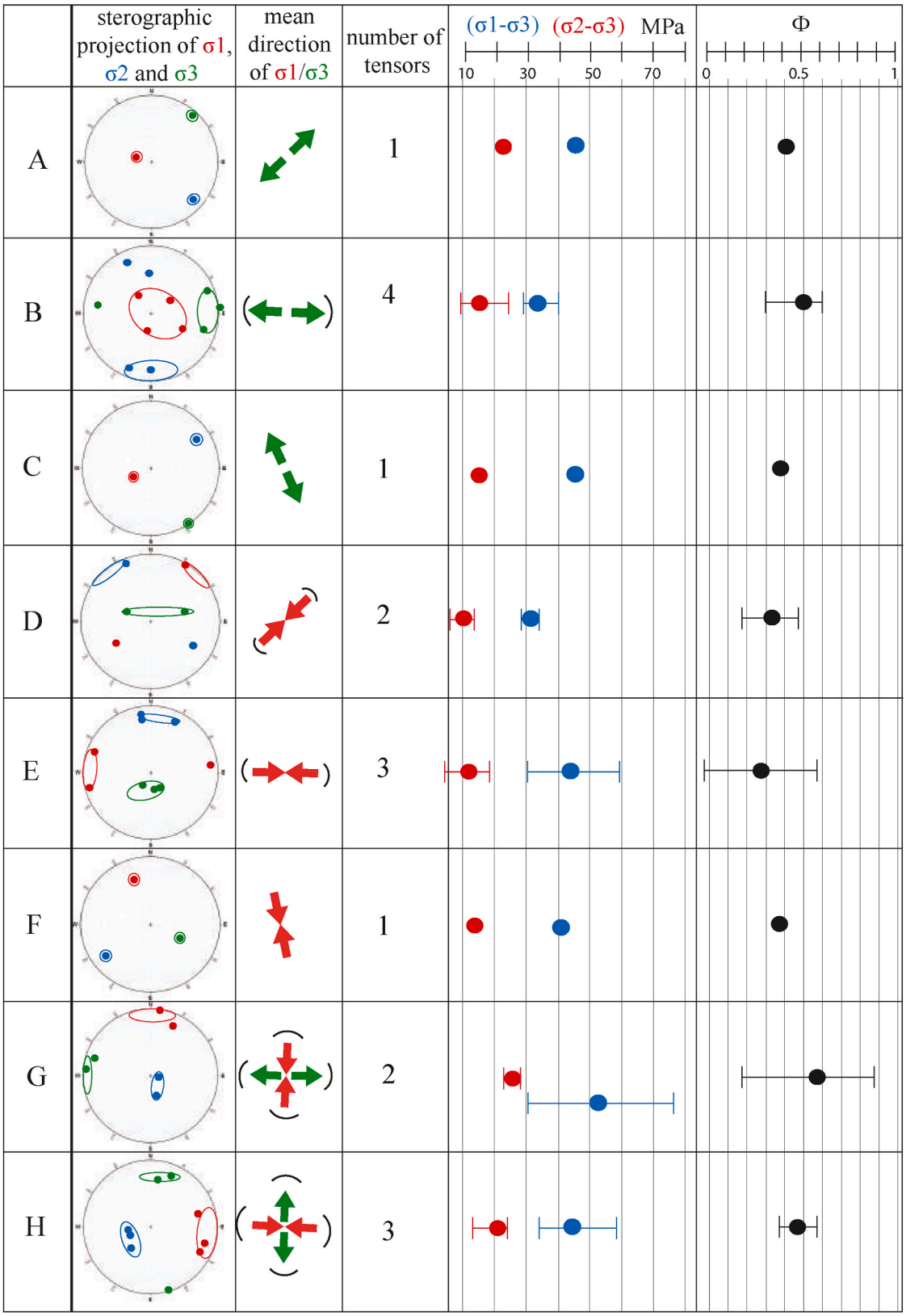

Fig. 11. Summary of stress tensor groups derived from calcite twin inversion using CSIT-2. Each tensor group (from A to H) is characterized by a plot data in stereographic equal-area projection showing the mean orientation of the principal stress axes (red for σ1, blue for σ2 and green for σ3) and the representation of the average orientation of the horizontal stresses as arrows (red for σ1, green for σ3, map view). Each tensor group is associated with the number of samples from which the related stress tensors were identified. The average values of the differential stress magnitudes for each group are shown in blue (σ1 - σ3) and in red (σ2 - σ3) and the average value of stress ratio Φ in black.

evidence of vertical σ_1 as indicated by active stylolitization are potentially periods when horizontal σ_1 was prevailing. This assumption constrains the possible timing of stress regimes with horizontal σ_1 (i.e. strike-slip and compressional states of stress) recorded by calcite twinning. The combination of calcite twin stress results with stylolite paleopiezometry together with the knowledge of basin-scale and core-scale fault patterns enabled us to propose a consistent sequence of regional (paleo)stress over time since the deposition of the syn-rift, pre-salt carbonates (Figs. 10 and 12).

5.1. Syn-rift extensional paleostresses in the Outer Kwanza basin

The estimated depths of pressure solution resulting from SRIT projected onto the burial model, along with the independently estimated age of the onset of rifting (Beglinger et al., 2012; Salomon et al., 2015), allow us to state that from ~130 Ma until at least ~57 Ma, the stress regime has been dominated by a vertical σ_1. Consequently, we constrain the extensional paleostresses recorded by calcite twinning (stress tensor groups A, B and C) between ~130-120 (the absolute age of dolomite considering uncertainties) and ~57 Ma, and more probably between 130 and ~112 Ma (end of rifting). From ~112 Ma to ~57 Ma, burial stress and related vertical compaction likely dominated, with no evidence of horizontal extension.

The strike and the kinematics of the regional normal faults structuring the sub-salt (Fig. 4A) and of the mesoscale faults from the cores of the pre-salt carbonates (Fig. 4B) provide evidence for polyphase extensional history during rifting. The normal faults striking N-S (black on Fig. 4A) to NNW-SSE (set 1 in Fig. 4B) are kinematically consistent with the stress tensor group B (~E-W extension), while the normal faults striking NW-SE (red in Fig. 4A) to WNW-ESE (set 3 in Fig. 4B) are compatible with the stress tensor group A (~NE-SW extension). Mesoscale normal faults striking NE-SW (set 2 in Fig. 4B) are kinematically compatible with the stress tensor group C (NNW-SSE extension) and with the few normal faults striking NE-SW (purple in Fig. 4A), but this fault strike is nearly absent at the regional scale and this state of stress was very rarely reconstructed from our dataset. The consistency of the extensional stress tensor groups A and B (and to a lesser extent C) with the kinematics of the normal fault and fracture pattern affecting the pre-salt carbonates in the offshore Kwanza basin confirms that these groups of tensors reflect extensional events associated with continental rifting between 130 and 112 Ma.

5.2. Post-rift strike-slip and compressional paleostresses in the Outer Kwanza basin

Our results show with confidence that σ_1 was no longer vertical after ~17 Ma. Consequently, a compressional or strike-slip state of stress (σ1 horizontal) has likely prevailed since then. The compressional and strike-slip stress tensor groups E and H are both associated with horizontal σ_1 oriented ENE-WSW to E-W, respectively. Since this σ_1 trend agrees with the regional present-day stress field (Fig. 1), and despite the trend of the σ_H derived from the borehole breakouts in the area investigated appears to be highly variable (unpublished internal report, TotalEnergies), we propose that a state of stress with horizontal σ_1 oriented ENE-WSW to E-W and with σ_2-σ_3 permutations prevailed from ~17 Ma until present.

The absence of strong constraints on the attitude of σ_1 during most of the period starting after ~57 Ma (time at which most of analyzed BPS having stopped their development) until ~17 Ma makes it possible to propose that the stress tensor groups associated with horizontal σ_1 oriented ~ N-S (to NE-SW) (groups D, F and G) could reflect a state of stress that prevailed either continuously or transiently during this period. The consistency of the reconstructed compressional trends with the latest Cretaceous (-early Paleocene) compression described by Guiraud and Bosworth (1997) leads us to assign a latest Cretaceous-early Paleocene age (~67–60 Ma) to the stress tensor groups D, F and G. This timing is in line with the onset of the decrease of burial rate at ~65 Ma as seen on the burial model. This timing is also roughly consistent with the end of activity of most (88%) of the analyzed stylolites at ~57 Ma when considering uncertainties (Fig. 10).

5.3. Comparison with the stress results and timing of deformation in the offshore Lower Congo basin

In the Outer Kwanza basin, the chronology of regional normal faults is difficult to establish. In the Lower Congo basin, the analysis of the distribution of the normal faults the dominant strike of which is changing according to the location (top Likouala high vs adjacent Dentale and Emeraude basins) led Bah et al. (2023a) to propose that the N-S striking normal faults predated the NE-SW normal faults. On this

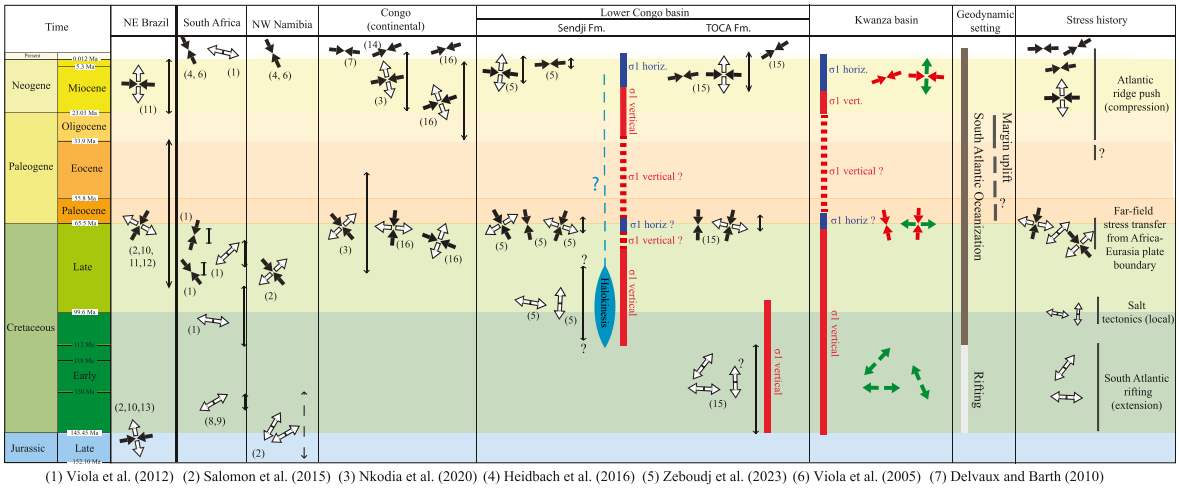

(1) Viola et al. (2012) (2) Salomon et al. (2015) (3) Nkodia et al. (2020) (4) Heidbach et al. (2016) (5) Zeboudj et al. (2023) (6) Viola et al. (2005) (7) Delvaux and Barth (2010) (8) Rabinovich and LaBrecque (1979) (9) Nurenberg and Muller (1991) (10) Ricomini (1995) (11) Fernandes and Amaral (2002) (12) Machado et al. (2012) (13) Ferrari (2001) (14) Nkodia et al. (2022)(15) Bah et al. (2023a) (16) Nkodia et al. (2024)

Fig. 12. Summary of the time distribution of tectonic events and associated stress orientations (projected onto the present position of Africa in map view) since early Cretaceous to present recorded in the southern West Africa (Congo, Namibia, Angola and South Africa) and Brazil. Stress data: (1) Viola et al. (2012) (2) Salomon et al. (2015) (3) Nkodia et al. (2020) (4) Heidbach et al. (2016) (5) Zeboudj et al. (2023) (6) Viola et al. (2005) (7) Delvaux and Barth (2010) (8) Rabinowitz and LaBrecque (1979) (9) Nurenberg and Müller (1991) (10) Riccomini (1995) (11) Fernandes and Amaral (2002) (12) Machado et al. (2012) (13) Ferrari (2001) (14) Nkodia et al. (2022) (15) Bah et al. (2023a) (16) Nkodia et al. (2024)

basis, the authors proposed that the extensional trend evolved from ~E-W to NE-SW probably during the Barremian. This sequence is consistent with the chronological observations which indicate that in the Outer Kwanza basin the mesoscale normal faults of set 3 postdate those of set 1 (Fig. 4B), but the record of the two extensional trends within the Barremo-Aptian pre-salt carbonates implies that the change from E-W to NE-SW might have occurred slightly later, during the late Barremian - early Aptian (?). The precise timing of the N-S to NNW-SSE extension in both the Lower Congo basin and the Outer Kwanza basin remains unconstrained.

The compressional trends derived from calcite twinning in the pre-salt carbonates in the Outer Kwanza basin and in the TOCA Fm in the Lower Congo basin are also similar, corresponding to a ~N-S and a ~E-W horizontal σ_1 (Fig. 12). Calcite twin analyses from the supra-salt Sendji Fm (Zeboudj et al., 2023) yield similar results on most of the post-rift paleostress record (Fig. 12). The major difference between the stress records in the two formations is that the supra-salt Sendji Fm recorded the post-rift halokinesis and related paleostresses that were (as expected) not recorded in the pre-salt TOCA Fm in the Lower Congo basin and the pre-salt carbonates in the Outer Kwanza basin.

The timing of the post-rift ~ N-S and ~E-W compressions was only loosely constrained by the study of the TOCA Fm by Bah et al. (2023a) who provided evidence that σ_1 remained vertical between 130 and 95 Ma. However, the timing of the ~E-W compressional trend was more tightly constrained by Zeboudj et al. (2023) in the Sendji Fm. Zeboudj et al. (2023) reported that most compaction-related stylolitization has been roughly active between 102 and 15 Ma. They therefore proposed to assign a post-15 Ma age to the state of stress with horizontal σ_1 oriented ~ E-W which is consistent with the present-day state of stress (Delvaux and Barth, 2010; Heidbach et al., 2018; Nkodia et al., 2022; Bah et al., 2023a: Fig. 1) This timing is consistent with the post ~17 Ma age inferred in the Kwanza basin (Fig. 10). For the ~N-S compressional trend, a late Cretaceous (-early Paleocene) age was similarly ascribed in the Outer Kwanza basin and in the Lower Congo basin mainly on the basis on directional correlation with the compression described by Guiraud and Bosworth (1997). It is noticeable that this timing fits also well with the 75-33 Ma time interval when the burial rate of the Sendji Fm slowed down (and activity of BPS under a vertical σ_1 transiently stopped ?) and the Sendji reservoir uplifted (Zeboudj et al., 2023).

5.4. Comparison with the stress results and timing of deformation in the onshore Congo basin

The history of brittle faulting and associated paleostress states has been investigated recently in the rapids of the Congo River at the outlet of the Pool Malebo (Fig. 1) between Kinshasa and Brazzaville by Nkodia et al. (2024). Faults and fractures collected there in the early Paleozoic Inkisi arkosic sandstones revealed a polyphase tectonic history and allowed reconstruction of four successive states of stress since Permian-Triassic times. The more recent fracturing event is related to a strike-slip to transtensional stress regime with a ENE-WSW (N070) horizontal σ1 which has been related to the mid-Atlantic ridge-push forces. This state of stress generated a dominant network of NE-SW trending fractures in the Inkisi arkoses. A prominent deformation zone consequently developed in the Pool area with a high density of fractures that merged together into long NE-SW fault zones. Nkodia et al. (2024) propose that the development of such suitably oriented NE-SW fault corridors had a marked imprint in the modern landscape and likely enabled the capture of the Congo basin drainage system by the Lower Congo river, connecting the hydrological system of the Congo basin to the Atlantic Ocean through the elevated Central African Atlantic swell (Mayombe Swell, Fig. 1). Because (1) in the Congo deep-sea fan, an early Oligocene major submarine erosion event has been evidenced before an important increase in terrigenous output (Anka et al., 2009; Lavier et al., 2001) and (2) a basal Oligocene unconformity has been identified along the West Africa margin (Teisserenc and Villemin, 1989; Anka et al., 2009), NKodia et al. (2024) propose that the onset of this deformation event corresponds to the sudden and massive resuming of sedimentation in the Congo deep-sea fan on the Atlantic sea floor at the beginning of the Oligocene (Fig. 12).

This age of the onset of the ENE-WSW to E-W compression at ~34 Ma contrasts with the age at ~15 Ma proposed by Zeboudj et al. (2023) in the Lower Congo basin and at ~17 Ma inferred in the Outer Kwanza basin (this study). In the Outer Kwanza basin, the (late Eocene-) Oligocene regional event of uplift/erosion was followed by a renewed high burial rate of the pre-salt carbonates starting in the early Miocene (~23 Ma, Fig. 10). If one considers that this renewed high rate of burial is related to sedimentation in the Congo deep-sea fan, it is possible that compaction-related pressure-solution under a vertical σ_1 was still active or, more likely, resumed during the (Oligocene-)early Miocene in response to increasing overburden (as possibly marked by the deepest stylolite on the distribution of Fig. 10), while the eroding onshore west Africa was already undergoing ENE-WSW to E-W compression. The delay in the record of this compressional trend in the offshore domain (at ~17-15 Ma) would be related to the time required for the tectonic-related horizontal σ_1 to overcome the burial-related vertical stress. As a result, our results do not rule out that the ENE-WSW to E-W oriented compressional stress could have prevailed from the Oligocene (~34 Ma) until the present (Fig. 12) as proposed by Nkodia et al. (2022).

Nkodia et al. (2024) also characterized the present-day stress field in the Congo basin tensor by inverting the focal mechanisms of 9 earthquakes in the Atlantic passive margin of Central African and the western margin of the Congo basin. The resulting stress tensor shows a horizontal σ_1 oriented ENE-WSW (N074°E) in a transpressional stress regime, slightly different from Nkodia et al. (2022) who obtained a pure compressional stress tensor with a σ_1 oriented N066°E. This result is consistent with the present-day N50° σ_H trends derived from borehole breakouts in the Lower Congo basin (Bah et al., 2023a) although the stress regime is rather strike-slip in type (Fig. 1). These results corroborate the idea that the ENE-WSW to E-W compression may have evolved in time and space (across and along the strike of the margin) between a strike-slip and a compressional stress regime.

From their analysis of the fracture and fault populations in the Pool area, NKodia et al. (2024) also documented three earlier states of stress (Fig. 12): a strike-slip state of stress associated with a horizontal σ_1 oriented N-S, which was also recognized in the Outer Kwanza basin and Lower Congo basin; a strike-slip state of stress associated with a horizontal σ_1 oriented WNW-ESE, and a strike-slip state of stress associated with a horizontal σ1 oriented NNW- SSE. The age of the two former stress events remains uncertain in the absence of any stratigraphic constraints, but on the basis of the consistency of the reconstructed compressional trends with those reported by Guiraud et al. (2005), Guiraud and Bosworth (1997) and Viola et al. (2012)(Fig. 12), these events were ascribed to the Late Maastrichtian and to the Late Santonian, respectively. The NNW-SSE compression was dated by NKodia et al. (2024) thanks to stratigraphic and petrological observations to the Permo-Triassic (~250 Ma) and is likely related to the Gondwanide subduction orogeny.

6. Tectonic evolution and paleostress history of the central segment of the West Africa passive margin

6.1. Consistency and complementarity of paleostress reconstructions at different locations

The comparison of the stress results in the offshore Lower Congo and Outer Kwanza basins and in the onshore Congo basin reveals that the paleostress record on the available core samples may be incomplete depending on the location of the investigated sites and the age of the investigated formations but at the same time, it demonstrates a good level of consistency (in terms of orientation, regime and timing) when the same states of stress are recognized at different places.

Our study shows a high level of consistency between the ~E-W, NE-SW and NNW-SSE rifting-related extensional stresses reconstructed from the syn-rift pre-salt carbonates – TOCA eq in the Outer Kwanza basin compared to the syn-rift TOCA Fm in the Lower Congo basin (Fig. 12). These extensional states of stress were not identified by Nkodia et al. (2024) onshore in the Pool area, the most probable reason being that this area was located too far from the locus of rifting-related extension (400 km inland from the Atlantic coast). The late (and still active) ENE-WSW to E-W compression was identified at all locations and in all (pre-, syn- and post-rift) formations, but with contrasting possible timings for its onset (~34 Ma vs 17-15 Ma)(Fig. 12). The late Maastrichtian-early Paleocene ~ N-S compression was also identified in all sites and all formations, with no or loose age constraints other than correlation with a recognized regional tectonic event. The Permo-Triassic state of stress could be recognized in the old pre-rift sequences of the Pool area but as expected, it was not recorded in the younger Cretaceous formations investigated offshore. The supra-salt Sendji Fm recorded post-rift extensional paleostresses related to (the paroxysm of) the thin-skinned, salt-related gravity tectonics in late Albian-Cenomanian times, while these paleostresses were not recorded in the pre-salt pre--rift Inkisi Fm and syn-rift TOCA Fm and equivalent (Figs. 12 and 13). The late Santonian N-S to NW-SE compression described by Guiraud and Bosworth (1997) and identified onshore by NKodia et al. (2024) has not been recorded by calcite twinning in the Lower Congo basin and the Outer Kwanza basin (Bah et al., 2023a; Zeboudj et al., 2023; this study) while being identified in Namibia and South Africa (Viola et al., 2012; Salomon et al., 2015). The reason for the non-recognition of this state of stress in the offshore domain, should it be methodological (difficulty to discriminate and separate stress tensors associated with close orientations and regimes using calcite twins) or regional (little or no stress transmission) remains unclear at this time.

Eventhough at none of the above-mentioned locations has a complete paleostress evolution been fully reconstructed, the synthesis of the distinctive stress records allows us to depict the more complete paleostress evolution of the West Africa passive margin to date (Fig. 12), providing important constraints on the tectonic evolution of the (Central segment of the) west Africa passive margin.

6.2. *Syn-rift extensional paleostresses and the extensional tectonic history of the West Africa passive margin*

Based on the results of sedimentary stylolite roughness inversion and the known age of the onset of rifting (Lehner and De Ruiter, 1977; Karner et al., 1997; Contrucci et al., 2004; Beglinger et al., 2012; Salomon et al., 2015), it can be stated that the stress regime of the pre-salt, syn-rift sequences (TOCA Fm and equivalent pre-salt carbonates) was dominated by a vertical σ1 from at least 130 Ma (and even since ~145 Ma considering the age of the onset of rifting) to at least ~67-60 Ma.

The NE-SW extension direction reconstructed in the offshore domain is consistent with that recorded onshore on the southern and western coasts of Africa (Viola et al., 2012; Salomon et al., 2015, Fig. 12). This NE-SW direction of extension is linked to the opening of the South

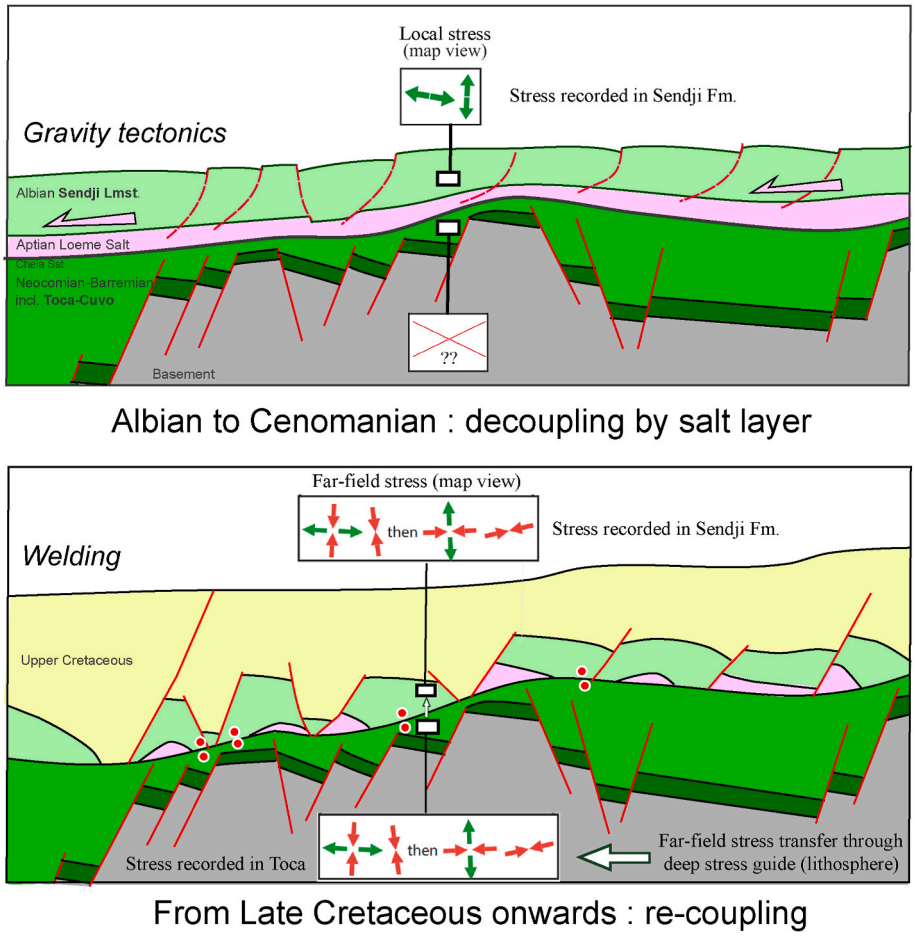

Fig. 13. Salt, basement-cover (de)coupling and stress transmission. Top, gravity sliding of the Sendji Fm above creeping salt. The supra-salt Sendji Fm recorded local extensional stresses while the pre-salt TOCA Fm and equivalent did not because of mechanical decoupling by the Loeme salt from the Albian to the Santonian (?). Bottom: Maastrichtian (-early Paleocene) and later stress regimes were consistently recorded in pre-salt and supra-salt formations, supporting that at least locally in the updip part of the slope of the passive margin, the salt decoupling level has welded and the sedimentary formations were mechanically recoupled to the basement, allowing for far-field lithospheric stress transmission to the entire sedimentary cover from below.

Atlantic ocean. The E-W extension that predated the NE-SW extension probably reflects a transient state of stress that preceded the main NE-SW extension (Fig. 12). These extensional trends are consistent with the pattern of regional N-S and NW-SE striking normal faults affecting the top of the TOCA Fm (Bah et al., 2023a) and eq TOCA pre-salt carbonates in the Outer Kwanza Basin (Fig. 4A) and with the distribution of mesoscale fractures reported in wells in the Outer Kwanza basin (Fig. 4B), the dominant NW-SE-striking normal faults being perpendicular to the main NE-SW (to ENE-WSW) direction of regional extension. Roughly similar extensional trends were recorded in Namibia (dominant ENE-WSW extension perpendicular to the continental margin and secondary NNE-SSW extension, Salomon et al., 2015) and South Africa (ENE-WSW extension, Viola et al., 2012) but were not in the Pool region of the onshore Congo basin (NKodia et al., 2024)(Fig. 12), indicating that extensional stresses were not transmitted far from the locus of extension (rift) in contrast to the far-field compressional stresses transferred from distant plate boundaries. The minor NNW-SSE (to N-S) extension, already described in the Lower Congo basin (Bah et al., 2023a), should reflect either a local transient stress permutation during regional extension or a local state of stress associated with a component of normal faulting along the ENE-WSW striking transfer faults (Bah et al., 2023a).

A possible reason for the observed change in extensional trends related to rifting (Fig. 12) pertains to structural inheritance. As already elaborated in Bah et al. (2023a), basement structures inherited from the formation of the Neoproterozoic Mayumbe belts (oriented NNW-SSE, Pedrosa-Soares et al., 1992; Affaton et al., 2016) and of the Kaoko belt (N-S trending foliation, e.g., Passchier et al., 2002; Goscombe and Gray, 2008) likely controlled the development of later extensional structures. These orogenic belts developed basement weaknesses favorably oriented for extensional reactivation under ~ E-W to NE-SW extension during subsequent rifting. The record of a ~E-W extension in the Outer Kwanza basin could be linked with the early development of N-S striking normal faults owing to the reactivation of N-S basement weaknesses, before NW-SE striking normal faults newly developed under the dominant regional NE-SW extension leading to the opening of the Atlantic ocean at this latitude. Alternatively, the change from E-W to NE-SW syn-rift extension in the Central segment of the West Africa margin could also be linked to a change in kinematic boundary conditions, i.e., the divergence between Africa and South America plates. The kinematic reconstructions by Heine et al. (2013) involve an E-W divergent motion between Africa and South America at 132 Ma changing to a NE-SW divergent motion at ~126 Ma. Considering the depositional age of the pre-salt carbonates and the age of the primary calcite matrix from which calcite twin measurements were taken, a change from ~E-W to NE-SW extension at ~126 Ma or slightly later would be consistent with both our paleostress results and the regional normal fault pattern in the Lower Congo basin and in the Outer Kwanza basin. Although we favor these two, not mutually exclusive explanations, a third explanation for the record of multiple extensional trends would consist in the combined effects of flexural bending due to post-rift sediment loading offshore and lithospheric doming above the continuous upwelling African superplume, causing a nearly radial pattern of gravitational extensional stresses (Salomon et al., 2015).

6.3. Post-rift (local) extensional paleostresses and thin-skinned, salt-related gravity tectonics of the West Africa passive margin

In the Lower Congo basin, Zeboudj et al. (2023) analyzed samples from cores of the deeply buried supra-salt Sendji Fm. The cores come from the N'Kossa raft structure, which is laying on a thin salt pillow of the late Aptian Loeme Fm and is bounded by major, N–S to NE-SW striking listric normal faults rooting within the Loeme salt. These normal faults mark a roughly E-W-oriented, salt-related and gravity-driven thin-skinned extensional deformation in the upslope domain of the margin mostly in late Albian to Cenomanian times. This extensional deformation is likely to be related to the gravitational movements of sediments sliding on the Loeme salt detachment level in the updip domain of the slope of the margin. This early gravity Albian updip deformation is characterized primarily by overburden extension with the development of disjointed rafts as a result of dismantling of the first post-salt sedimentary formations (e.g., Sendji Fm), with the gaps between the divergent rafts being filled in by late Cretaceous formations like the Cenomanian Likouala Fm.

From their analysis of calcite twins, Zeboudj et al. (2023) reported extensional stress regimes with σ_3 trending ~ N–S and ~E-W (Fig. 12). The E-W extension was likely related to the activity of the major N-S striking thin-skinned normal faults. The sub-perpendicular ~ N-S extension was related to the complex pattern of interconnected normal faults and to the vicinity of the well with the northern boundary of the N'Kossa raft structure which corresponds to a roughly NE-SW to E-W oriented free edge favoring gravity-driven extension nearly perpendicular to it. The authors concluded that these two extensional stress regimes were of local significance in that they were restricted to the detached supra-salt cover (Fig. 13), and associated with salt tectonics from 110 to 80 Ma. In that sense, the salt acted as an efficient decoupling level between the supra-salt and the infra-salt formations and deeper crust resulting in a different paleostress record and structural pattern between the post-rift, supra-salt Sendji Fm (Zeboudj et al., 2023) and the infra-salt, syn-rift TOCA and equivalent (Bah et al., 2023a; this study) (Fig. 12). Despite being of considerable importance in shaping the margin and despite the link between salt distribution and rifted margin architecture/salt-base relief (Evans and Jackson, 2019; Pichel et al., 2023), this thin-skinned extension does not reflect any crustal extension at that time.

6.4. Post-rift compressional/strike-slip paleostresses and the far-field stress transfer from distant plate boundaries

During the post-rift evolution of the West African passive margin, several states of stress, either strike-slip or compressional in type, have been recorded along its central segment (Lower Congo and Outer Kwanza basins), and even more to the south (Namibia and South Africa) (Fig. 12).

Although not recognized (or identified as such) in cores from the offshore domain (Bah et al., 2023a; Zeboudj et al., 2023; this study), a strike-slip stress regime associated with σ_1 oriented WNW-ESE to NW-SE was reported in South Africa (Viola et al., 2012), Namibia (Salomon et al., 2015) and continental Congo (Nkodia et al., 2020, 2024)(Fig. 12). In the absence of stratigraphic constraints, this state of stress has been related to the late Santonian (N-S to) NW-SE compression described in Central and North Africa by Guiraud and Bosworth (1997)(Fig. 12). After a short extensional event that was only reported by Viola et al. (2012), a strike-slip/compressional stress regime associated with σ_1 ~N-S to NNE-SSW has been widely recognized. The age of this event remains loosely constrained but all authors agree with the idea that it most probably corresponds to the latest Maastrichtian-early Paleocene (~67-60 Ma) N-S to NNE-SSW compression described by Guiraud and Bosworth (1997)(Fig. 12).

The record all along the western coast of Africa as far in south Africa, including in the offshore domain, of the late Santonian and/or the late Maastrichtian-early Paleocene compressions recognized in northern and Central Africa and interpreted by Guiraud and Bosworth (1997) as related to a plate reorganization during the Alpine cycle and to the shift in the spreading directions of the Atlantic ocean and the subsequent counter clockwise rotational northward drift of Africa-Arabia into Eurasia implies a far-field stress transfer from the distant Africa-Eurasia plate boundary. Such far-field stress transfer likely required an efficient deep stress guide, i.e., a high strength African continental lithosphere.

Interestingly, the record of the ~N-S compressional trend both in the pre-salt TOCA and equivalent formations and in the supra-salt Sendji Fm

supports that these formations were no longer mechanically decoupled in the latest Cretaceous-early Paleocene but instead that the detachment layer was, at least locally, welded, likely due to the nearly complete salt removal at that time in the proximal (updip) domain of the margin (Zeboudj et al., 2023), so the entire sedimentary cover became able to record the far-field lithospheric compressional stress (Fig. 13).

Later on, strike-slip and compressional stress regimes with horizontal σ_1 trending ENE-WSW to E-W possibly dominated since the early Oligocene while being not recorded offshore with certainty before the Miocene (~17-15 Ma). This ENE-WSW to E-W trend is nearly perpendicular to both the continental passive margin and the mid-Atlantic ridge (Fig. 1). Following Bah et al. (2023a), Zeboudj et al. (2023) and NKodia et al. (2022, 2024), we propose that this compressional trend be related to a far-field effect of the mid-Atlantic ridge push, prevailing from the Oligocene-Miocene onwards. This interpretation reinforces the concept that the ridge push could efficiently influence the long-lived state of stress in (the upper part of) the lithosphere (e.g., Wiens and Stein, 1983, 1985) and that the gravitational compressional stresses related to the Atlantic ridge push may be transferred far into the interior of the oceanic and continental parts of the African plate (Mahatsente and Coblentz, 2015).

The interpretation of the post-rift strike-slip and compressional paleostresses in term of far-field stress transfer is in line with earlier findings by Withjack et al. (1995) who reported that during the development of a passive margin, rift basins may have experienced shortening possibly associated with sea-floor spreading processes such as ridge push or continental resistance to plate motion. It further corroborates the conclusions of Vagnes et al. (1998) that the Norwegian Atlantic passive margin underwent late Cretaceous–Cenozoic intraplate contractional deformation possibly related to far-field effects of Alpine active plate-margin processes, with additional significant contribution of ridge push from the North Atlantic spreading particularly during Neogene times.

At the present day, a compression oriented from ENE-WESW to E-W has been identified on the eastern margin of the South Atlantic ocean (Ziegler et al., 1995; Delvaux and Barth, 2010; Heidbach et al., 2018; Schirbel et al., 2024)(Fig. 1). In the Central segment of the margin investigated in this study, available current stress data from earthquake focal mechanism and borehole breakouts indicate a dominant σ_H oriented ENE-WSW to E-W in a compressional or a strike-slip stress regime (Fig. 1). In the offshore Republic of Congo, borehole breakouts reveal a σ_H oriented N50° in a strike-slip stress regime (unpublished TotalEnergies report, Fig. 1). The inversion of earthquake focal mechanisms (Heidbach et al., 2018; Nkodia et al., 2022, 2024) reveals a strike-slip to compressional stress regime with σ_H oriented ~ N70 in offshore Angola in the Lower Congo basin that progressively switches to a strike-slip stress regime with a σ_H oriented N80 to N100-120 (ENE-WSW to WNW- ESE) in the interior of the Congo basin (Nkodia et al., 2022), and a compressional stress regime with a σ_H oriented ~ N80 in the interior Gabon (Fig. 1). A recent study of induced seismicity in the Lauca reservoir in the Angola craton revealed a σ_H oriented ~ ENE-WSW (N57) in a strike-slip stress regime (Schirbel et al., 2024)(Fig. 1). These results all point to a modern strike-slip or compressional state of stress with a σ_H trend ranging from NE-SW to E-W nearly perpendicular to both the continental passive margin and the mid-Atlantic ridge in the Central segment of the West Africa margin, likely dominantly controlled, like the Neogene stress, by a far-field effect of the mid-Atlantic ridge push. The record of a far-field transfer of compressional stresses related to the ridge push into the continental part of the African (Nubian) plate since the Oligocene requires that the strength of the Atlantic oceanic lithosphere be larger than the ridge-push force so there is no significant stress dissipation by intraplate deformation; numerical models show that this behavior is compatible with a dry rheology of the oceanic lithosphere (Mahatsente, 2017). The fact that this σ_H (=σ_1) trend is related either to strike-slip, transpressional or compressional regimes depending on the location points to probable local σ_2- σ_3 stress permutations in space possibly related to structural complexities (e.g., Hu and Angelier, 2004) as already proposed by Bah et al. (2023a), changes in elevation (e.g., Schirpel et al., 2024) or to a weak difference in magnitude between σ_2 and σ_3.

It is worth noting that we cannot rule out that other stress sources involved throughout the African plate, such as density variations within the lithosphere or flexural loading of the lithosphere may have contributed to the late Tertiary and present-day stress fields along the West Africa passive margin (e.g., Medvedev, 2016).

7. Conclusions

In this paper, we adopted an integrated approach which combines burial modelling with inversion of calcite twins for tectonic stress, inversion of sedimentary stylolite roughness for burial stress and analysis of fault and fracture networks to reconstruct the paleostress history of the Outer (offshore) Kwanza basin from cores from three deep industrial wells.

Three main tectonic events affected the pre-salt carbonate sequences during their burial history: (1) rifting-associated extension between 130 and 112 Ma, with σ_3 evolving from ~E-W to NE-SW; (2) intraplate ~ N-S compression, possibly dated at ~67-60 Ma and reflecting a far-field transfer of orogenic stress from the distant Africa-Eurasia active plate boundary; (3) intraplate ENE-WSW to E-W compression that we propose to mostly relate to the mid-Atlantic ridge push from at least ~17-15 Ma onwards and possibly since ~34 Ma.

Together with earlier paleostress reconstructions, our results demonstrate that the West Africa passive margin underwent a polyphase tectonic history, including multiple syn-rift extensions and post-rift compressions. Except local shallow post-rift stress associated with salt tectonics (e.g., updip extension in response to gravity sliding above salt) in salt-bearing segments, most reconstructed post-rift states of stress are strike-slip and compressional in type and originated from far-field either tectonic or gravitational lithospheric stress transferred from distant active plate boundaries. We believe this conclusion can safely be extended to many other passive margin worldwide.

CRediT authorship contribution statement

Boubacar Bah: Writing – review & editing, Writing – original draft, Visualization, Validation, Investigation, Formal analysis, Conceptualization. **Olivier Lacombe:** Writing – review & editing, Writing – original draft, Visualization, Validation, Supervision, Project administration, Investigation, Funding acquisition, Data curation, Conceptualization. **Nicolas E. Beaudoin:** Writing – review & editing, Writing – original draft, Visualization, Validation, Software, Methodology, Investigation, Formal analysis, Conceptualization. **Pierre-Alexandre Teboul:** Writing – review & editing, Writing – original draft, Visualization, Supervision. **Jean-Pierre Girard:** Writing – review & editing, Writing – original draft, Visualization, Validation, Supervision, Methodology, Investigation. **Claude Gout:** Writing – review & editing, Writing – original draft, Visualization, Validation, Supervision, Software, Methodology, Investigation, Funding acquisition.

Declaration of competing interest

The authors declare that they have no conflict of interest to disclose.

Data availability

Data will be made available on request.

Acknowledgments

The authors are very grateful to TotalEnergies and Angola subsidiary for granting financial support to this research, for providing the cores

and prior data, and for permission to publish. NEB is funded through the isite-E2S, supported by the ANR PIA and the Région Nouvelle-Aquitaine. The U–Pb dating analyses were carried out as part of a collaborative R&D project (DATCARB) between CEREGE and TotalEnergies (2018–2021), co-funded by the "Excellence Initiative" program of Aix Marseille University A*MIDEX, TotalEnergies, and Sud region. Abel Guihou is thanked for his technical support in the U–Pb analyses by LA-ICPMS. The authors also acknowledge the useful comments by Nuretdin Kaymakci and an anonymous reviewer.

Appendix A. Supplementary data

Supplementary data to this article can be found online at https://doi.org/10.1016/j.jafrearsci.2024.105382.

References

Aharonov, E., Katsman, R., 2009. Interaction between pressure-solution and clays in stylolite development: insights from modeling. Am. J. Sci. 309 (7), 607–632.
Affaton, P., Kalsbeek, F., Boudzoumou, F., Trompette, R., Thrane, K., Frei, R., 2016. The pan-African west Congo belt in the republic of Congo (Congo Brazzaville): stratigraphy of the mayombe and west Congo supergroups studied by detrital zircon geochronology. Precambrian Res. 272, 185–202.
Amrouch, K., Lacombe, O., Bellahsen, N., Daniel, J.-M., Callot, J.P., 2010. Stress and strain patterns, kinematics and deformation mechanisms in a basement-cored anticline: sheep Mountain anticline (Wyoming, USA). Tectonics 29, TC1005.
Amrouch, K., Beaudoin, N., Lacombe, O., Bellahsen, N., Daniel, J.M., 2011. Paleostress magnitudes in folded sedimentary rocks. Geophys. Res. Lett. 38, L17301.
Anka, Z., Séeranne, M., Lopez, M., Schreck-Wenderoth, M., Savoye, B., 2009. The long-term evolution of the Congo deep-sea fan: a basin-wide view of the interaction between a giant submarine fan and a mature passive margin (ZaiAngo project). Tectonophysics 470, 42–56.
Atashbari, V., Tingay, M., 2012. Pore pressure prediction in carbonate reservoirs. In: SPE Latin America and Caribbean Petroleum Engineering Conference. OnePetro Conference. April 2012.
Arboit, F., Amrouch, K., Collins, A.S., King, R., Morley, C., 2015. Determination of the tectonic evolution from fractures, faults, and calcite twins on the southwestern margin of the Indochina Block. Tectonics 34, 1576–1599.
Aslanian, D., Moulin, M., Olivet, J.L., Unternehr, P., Matias, L., Bache, F., Rabineau, M., Klingelheofer, F., Contrucci, I., Labails, C., 2009. Brazilian and African passive margins of the central segment of the South Atlantic Ocean: kinematic constraints. Tectonophysics 468 (1–4), 98–112.
Asmus, H.E., Ponte, F.C., 1973. The Brazilian marginal basins. In: The South Atlantic. Springer, Boston, MA, pp. 87–133.
Bah, B., Beaudoin, N.E., Lacombe, O., Girard, J.-P., Gout, C., Godeau, N., Deschamps, P., 2023b. Multi-proxy reconstruction of the burial history and porosity evolution of the TOCA carbonate formation in the Lower Congo basin (South West Africa). Mar. Petrol. Geol. 148, 106018.
Bah, B., Lacombe, O., Beaudoin, N., Zeboudj, A., Gout, C., Girard, J.-P., Teboul, P.-A., 2023a. Paleostress evolution of the West African passive margin: new insights from calcite twinning paleopiezometry in the deeply buried syn-rift TOCA formation (Lower Congo basin). Tectonophysics 863, 22997.
Bate, R.H., 1999. Non-marine ostracod assemblages of the Pre-Salt rift basins of West Africa and their role in sequence stratigraphy. Geological Society, London, Special Publications 153 (1), 283–292.
Bate, R.H., Cameron, N.R., Brandao, M.G.P., 2001. The lower cretaceous (Pre-Salt) lithostratigraphy of the Kwanza Basin, Angola. Newslett. Stratigr. 38, 117–127.
Beaudoin, N., Lacombe, O., 2018. Recent and future trends in paleopiezometry in the diagenetic domain: insights into the tectonic paleostress and burial depth history of fold-and-thrust belts and sedimentary basins. J. Struct. Geol. 114, 357–365.
Baudouy, S., Legorjus, C., 1991. Sendji field–People's Republic of Congo, Congo Basin, pp. 121–149.
Beaudoin, N., Gasparrini, M., David, M.E., Lacombe, O., Koehn, D., 2019. Bedding-parallel stylolites as a tool to unravel maximum burial depth in sedimentary basins: application to Middle Jurassic carbonate reservoirs in the Paris basin, France. Geol. Soc. Am. Bull. 131 (7–8), 1239–1254.
Beaudoin, N., Lacombe, O., Koehn, D., David, M.E., Farrell, N., Healy, D., 2020a. Vertical stress history and paleoburial in foreland basins unravelled by stylolite roughness paleopiezometry: insights from bedding-parallel stylolites in the Bighorn Basin, Wyoming, USA. J. Struct. Geol. 136, 104061.
Beaudoin, N., Labeur, A., Lacombe, O., Koehn, D., Billi, A., Hoareau, G., Boyce, A., John, C.M., Marchegiano, M., Roberts, N.M., Millar, I.L., Claverie, F., Pecheyran, C., Callot, J.-P., 2020b. Regional-scale paleofluid system across the Tuscan Nappe – umbria Marche Arcuate Ridge (northern Apennines) as revealed by mesostructural and isotopic analyses of stylolite-vein networks. Solid Earth 11, 1617–1641.
Beaudoin, N., Koehn, D., Lacombe, O., Lecouty, A., Billi, A., Aharonov, E., Parlangeau, C., 2016. Fingerprinting stress: stylolite and calcite twinning paleopiezometry revealing the complexity of progressive stress patterns during folding-The case of the Monte Nero anticline in the Apennines, Italy. Tectonics 35, 1687–1712.
Beglinger, S.E., Doust, H., Cloetingh, S., 2012. Relating petroleum system and play development to basin evolution: west African South Atlantic basins. Mar. Petrol. Geol. 30 (1), 1–25.
Bertotti, G., de Graaf, S., Bisdom, K., Oskam, B., Vonhof, H.B., Bezerra, F.H.R., Reijmer, J.J.G., Cazarin, C.L., 2017. Fracturing and fluid-flow during post-rift subsidence in carbonates of the Jandaíra formation, Potiguar basin, NE Brazil. Basin Res. 29 (6), 836–853.
Bott, M.H.P., 1993. Modelling the plate-driving mechanism. J. Geol. Soc. 150 (5), 941–951.
Brandstätter, J., Kurz, W., Rogowitz, A., 2017. Microstructural analysis and calcite piezometry on hydrothermal veins: insights into the deformation history of the Cocos Plate at Site U1414 (IODP Expedition 344). Tectonics 36 (8), 1562–1579.
Brice, S.E., Cochran, M.D., Pardo, G., Edwards, A.D., 1982. Tectonics and sedimentation of the South Atlantic Rift Sequence: cabinda, Angola: rifted margins: field investigations of margin structure and stratigraphy. In: Studies in Continental Margin Geology. AAPG Special Volumes, pp. 5–18.
Brownfield, M.E., Charpentier, R.R., 2006. Geology and Total Petroleum Systems of the West-Central Coastal Province (7203), 2207-B. United States Geological Survey Bulletin, West Africa, p. 52.
Burkhard, M., 1993. Calcite twins, their geometry, appearance and significance as stress-strain markers and indicators of tectonic regime: a review. J. Struct. Geol. 15 (3–5), 351–368.
Burov, E., Gerya, T., 2014. Asymmetric three-dimensional topography over mantle plumes. Nature 513 (7516), 85–89.
Burwood, R., 1999. Angola: source rock control for Lower Congo Coastal and Kwanza Basin petroleum systems. Geological Society, London, Special Publications 153 (1), 181–194.
Chaboureau, A.C., Guillocheau, F., Robin, C., Rohais, S., Moulin, M., Aslanian, D., 2013. Paleogeographic evolution of the central segment of the South Atlantic during Early Cretaceous times: paleotopographic and geodynamic implications. Tectonophysics 604, 191–223.
Cloetingh, S., Burov, E., Matenco, L., Beekman, F., Roure, F., Ziegler, P.A., 2013. The Moho in extensional tectonic settings: insights from thermo-mechanical models. Tectonophysics 609, 558–604.
Comin-Chiaramonti, P., De Min, A., Girardi, V.A.V., Ruberti, E., 2011. Post-Paleozoic magmatism in Angola and Namibia: a review. In: Beccaluva, L., Bianchini, G., Wilson, M. (Eds.), Volcanism and Evolution of the African Lithosphere, 478. Geological Society of America special paper, pp. 223–247.
Contrucci, I., Matias, L., Moulin, M., Géli, L., Klingelhofer, F., Nouzé, H., Aslanian, D., Olivet, J.L., Réhault, J.P., Sibuet, J.C., 2004. Deep structure of the West African continental margin (Congo, Zaïre, Angola), between 5°S and 8°S, from reflection/refraction seismics and gravity data. Geophys. J. Int. 158 (2), 529–553.
Craddock, J.P., Jackson, M., van der Pluijm, B.A., Versical, R.T., 1993. Regional shortening fabrics in eastern north America: far-field stress transmission from the appalachian-ouachita orogenic belt. Tectonics 12 (1), 257–264.
Craddock, J.P., Farris, D.W., Roberson, A., 2004. Calcite-twinning constraints on stress-strain fields along the Mid-Atlantic Ridge, Iceland. Geology 32 (1), 49–52.
Craddock, J.P., Liu, J., Zheng, Y., 2018. Twinning strains in synfolding calcite, proterozoic sinian system, China. Geosciences 8, 131.
Craddock, J.P., Princen, M., Wartman, J., Xia, H., Liu, J., 2016. Calcite twinning in the ordovician martinsburg formation, DelawarenWater gap, New Jersey, USA: implications for cleavage formation and tectonic shortening in the appalachian piedmont province. Geosciences 6, 10.
Davison, I., 2007. Geology and tectonics of the South Atlantic Brazilian salt basins. In: Geological Society, 272. Special Publications, London, pp. 345–359, 1.
Delvaux, D., Maddaloni, F., Tesauro, M., Braitenberg, C., 2021. The Congo Basin: stratigraphy and subsurface structure defined by regional seismic reflection, refraction and well data. Global Planet. Change 198 (2), 103407.
Delvaux, D., Barth, A., 2010. African stress pattern from formal inversion of focal mechanism data. Tectonophysics 482 (1–4), 105–128.
Duval, B., Cramez, C., Jackson, M.P.A., 1992. Raft tectonics in the Kwanza Basin, Angola. Mar. Petrol. Geol. 9 (4), 389–404.
Ebner, M., Koehn, D., Toussaint, R., Renard, F., Schmittbuhl, J., 2009. Stress sensitivity of stylolite morphology. Earth Planet Sci. Lett. 277 (3–4), 394–398.
Erdi, A., Jackson, C.A.L., 2021. What controls salt-detached contraction in the translational domain of the outer Kwanza Basin, offshore Angola? Basin Res. 33 (3), 1880–1905.
Evans, S.L., Jackson, C.A.L., 2019. Base-salt relief controls salt-related deformation in the Outer Kwanza Basin, offshore Angola. Basin Res. 32 (4), 668–687.
Fernandes, A.J., Amaral, G., 2002. Cenozoic tectonic events at the border of the Paraná basin, são paulo, Brazil. J. S. Am. Earth Sci. 14, 911–931.
Ferrari, A.L., 2001. Evolução Tectônica do Graben da Guanabara (PhD thesis. Instituto de Geociências da Universidade de São Paulo, p. 412.
Ferrill, D.A., 1998. Critical re-evaluation of differential stress estimates from calcite twins in coarse-grained limestone. Tectonophysics 285, 77–86.
Ferrill, D.A., Morris, A.P., Evans, M.A., Burkhard, M., Groshong Jr, R.H., Onasch, C.M., 2004. Calcite twin morphology: a low-temperature deformation geothermometer. J. Struct. Geol. 26 (8), 1521–1529.
Godeau, N., Deschamps, P., Guihou, A., Leonide, P., Tendil, A., Gerdes, A., Hamelin, B., Girard, J.P., 2018. U-Pb dating of calcite cement and diagenetic history in microporous carbonate reservoirs: case of the Urgonian Limestone. France. Geology 46 (3), 247–250.
Goscombe, B.D., Gray, D.R., 2008. Structure and strain variation at mid-crustal levels in a transpressional orogen: a review of Kaoko Belt structure and the character of West Gondwana amalgamation and dispersal. Gondwana Res. 13, 45–85.

Gradstein, F.M., Ogg, J.G., Smith, A.G., Bleeker, W., Lourens, L.J., 2004. A new geologic time scale, with special reference to Precambrian and Neogene. Episodes 27 (2), 83–100.
Grosdidier, E., Braccini, E., Dupont, G., Moron, J.M., 1996. Biozonation du Crétacé Inférieur non marin des bassins du Gabon et du Congo. In: Bulletin des Centres de recherches exploration-production Elf-Aquitaine, 16. Memoir, pp. 67–82.
Guiraud, R., Bosworth, W., 1997. Senonian basin inversion and rejuvenation of rifting in Africa and Arabia: synthesis and implications to plate-scale tectonics. Tectonophysics 282 (1–4), 39–82.
Guiraud, R., Bosworth, W., Thierry, J., Delplanque, A., 2005. Phanerozoic geological evolution of northern and central Africa: an overview. J. Afr. Earth Sci. 43 (1–3), 83–143.
Guiraud, M., Buta-Neto, A., Quesne, D., 2010. Segmentation and differential post-rift uplift at the Angola margin as recorded by the transform-rifted Benguela and oblique-to-orthogonal-rifted Kwanza basins. Mar. Petrol. Geol. 27 (5), 1040–1068.
Hadi, F., Nygaard, R., 2023. Estimating unconfined compressive strength and Young's modulus of carbonate rocks from petrophysical properties. Petrol. Sci. Technol. 41 (13), 1367–1389.
Harris, J.H., Van der Pluijm, B.A., 1998. Relative timing of calcite twinning strain and fold-thrust belt development: hudson Valley fold-thrust belt, New York, USA. J. Struct. Geol. 20, 21–31.
Harris, N.B., 2000. TOCA Carbonate, Congo Basin: response to an evolving rift lake. In: Mello, M.R., Katz, B.J. (Eds.), Petroleum Systems of South Atlantic Margins, 73. American Association of Petroleum Geologists Memoir, pp. 341–360.
Heidbach, O., Rajabi, M., Cui, X., Fuchs, K., Müller, B., Reinecker, J., Reiter, K., Tingay, M., Wenzel, F., Xie, F., Ziegler, M.O., Zoback, M.-L., Zoback, M.D., 2018. The World Stress Map database release 2016: crustal stress pattern across scales. Tectonophysics 744, 484–498.
Heidbach, O., Rajabi, M., Reiter, K., Ziegler, M., 2016. World stress map database release 2016. GFZ Data Services 10, 1.
Heine, C., Zoethout, J., Müller, R.D., 2013. Kinematics of the South atlantic rift. Solid Earth 5 (1), 41–116.
Hou, Z., Fusseis, F., Schöpfer, M., Grasemann, B., 2023. Synkinematic evolution of stylolite porosity. J. Struct. Geol. 173, 104916.
Hu, J.C., Angelier, J., 2004. Stress permutations: three-dimensional distinct element analysis accounts for a common phenomenon in brittle tectonics. J. Geophys. Res. Solid Earth 109 (B9).
Hudec, M.R., Jackson, M.P.A., 2004. Regional restoration across the Kwanza Basin, Angola: salt tectonics triggered by repeated uplift of a metastable passive margin. AAPG (Am. Assoc. Pet. Geol.) Bull. 88 (7), 971–990.
Hudec, M.R., Jackson, M.P.A., 2002. Structural segmentation, inversion, and salt tectonics on a passive margin: evolution of the Inner Kwanza Basin, Angola. Geol. Soc. Am. Bull. 114 (10), 1222–1244.
Jackson, M., Hudec, M., 2009. Interplay of basement tectonics, salt tectonics, and sedimentation in the Kwanza Basin, Angola. In: AAPG search and discovery article 30091, presented at the AAPG international conference and exhibition. AAPG Search and Discovery, p. 29.
Jamison, W.R., Spang, J.H., 1976. Use of calcite twin lamellae to infer differential stress. Geol. Soc. Am. Bull. 87 (6), 868–872.
Ji, S., Li, L., Motra, H.B., Wuttke, F., Sun, S., Michibayashi, K., Salisbury, M.H., 2018. Poisson's ratio and auxetic properties of natural rocks. Journal ofGeophysical Research: Solid Earth 123, 1161–1185.
Karl, M., Glasmacher, U.A., Kollenz, S., Franco-Magalhaes, A.O.B., Stockli, D.F., Hackspacher, P.C., 2013. Evolution of the South Atlantic passive continental margin in southern Brazil derived from zircon and apatite (U–Th–Sm)/He and fission-track data. Tectonophysics 604, 224–244.
Karner, G.D., Driscoll, N.W., McGinnis, J.P., Brumbaugh, W.D., Cameron, N.R., 1997. Tectonic significance of syn-rift sediment packages across the Gabon-cabinda continental margin. Mar. Petrol. Geol. 14 (7), 973–1000.
Karner, G.D., Driscoll, N.W., 1999. Tectonic and stratigraphic development of the West African and eastern Brazilian Margins: insights from quantitative basin modelling. Geological Society, London, Special Publications 153 (1), 11–40.
Karner, G.D., Gambôa, L.A.P., 2007. Timing and origin of the South Atlantic pre-salt sag basins and their capping evaporites. Geological Society, London, Special Publications 285 (1), 15–35.
Koehn, D., Renard, F., Toussaint, R., Passchier, C.W., 2007. Growth of stylolite teeth patterns depending on normal stress and finite compaction. Earth Planet Sci. Lett. 257, 582–595.
Koehn, D., Koehler, S., Toussaint, R., Ghani, I., Stollhofen, H., 2022. Scaling analysis, correlation length and compaction estimates of natural and simulated stylolites. J. Struct. Geol., 104670
Koehn, D., Ebner, M., Renard, F., Toussaint, R., Passchier, C.W., 2012. Modelling of stylolite geometries and stress scaling. Earth Planet Sci. Lett. 341, 104–113.
Koptev, A., Burov, E., Gerya, T., Le Pourhiet, L., Leroy, S., Calais, E., Jolivet, L., 2018. Plume-induced continental rifting and break-up in ultra-slow extension context: insights from 3D numerical modeling. Tectonophysics 746, 121–137.
Kukla, P.A., Strozyk, F., Mohriak, W.U., 2018. South Atlantic salt basins–witnesses of complex passive margin evolution. Gondwana Res. 53, 41–57.
Kulikowski, D., Amrouch, K., 2017. Combining geophysical data and calcite twin stress inversion to refine the tectonic history of subsurface and offshore provinces: a case study on the Cooper-Eromanga Basin, Australia. Tectonics 36 (3), 515–541.
Labeur, A., Beaudoin, N.E., Lacombe, O., Emmanuel, L., Petracchini, L., Daëron, M., Klimowicz, S., Callot, J.P., 2021. Burial-deformation history of folded rocks unraveled by fracture analysis, stylolite paleopiezometry and vein cement geochemistry: a case study in the Cingoli Anticline (Umbria-Marche, Northern Apennines). Geosciences 11 (3), 135.
Labeur, A., Beaudoin, N., Lacombe, O., Gout, C., Callot, J.P., 2024. Constraining the onset of orogenic contraction in fold-and-thrust belts using sedimentary stylolite populations (Umbria-Marche Apennines, Italy). J. Struct. Geol. 182, 105098.
Lacombe, O., Angelier, J., Laurent, P., Bergerat, F., Tourneret, C., 1990. Joint analyses of calcite twins and fault slips as a key for deciphering polyphase tectonics: burgundy as a case study. Tectonophysics 182 (3–4), 279–300.
Lacombe, O., Laurent, P., Angelier, J., 1994. Calcite twins as a key to paleostresses in sedimentary basins: preliminary results from drill cores of the Paris basin. In: Roure, F. (Ed.), Peri-Tethyan Platforms. Technip, pp. 197–210.
Lacombe, O., Laurent, P., 1996. Determination of deviatoric stress tensors based on inversion of calcite twin data from experimentally deformed monophase samples: preliminary results. Tectonophysics 255 (3–4), 189–202.
Lacombe, O., 2001. Paleostress magnitudes associated with development of mountain belts: insights from tectonic analyses of calcite twins in the Taiwan Foothills. Tectonics 20 (6), 834–849.
Lacombe, O., 2007. Comparison of paleostress magnitudes from calcite twins with contemporary stress magnitudes and frictional sliding criteria in the continental crust: mechanical implications. J. Struct. Geol. 29 (1), 86–99.
Lacombe, O., Amrouch, K., Mouthereau, F., Dissez, L., 2007. Calcite twinning constraints on late Neogene stress patterns and deformation mechanisms in the active Zagros collision belt. Geology 35 (3), 263–266.
Lacombe, O., Malandain, J., Vilasi, N., Amrouch, K., Roure, F., 2009. From paleostresses to paleoburial in fold-thrust belts: preliminary results from calcite twin analysis in the outer Albanides. Tectonophysics 475, 128–141.
Lacombe, O., 2010. Calcite twins, a tool for tectonic studies in thrust belts and stable orogenic forelands. Oil and Gas Science and Technology–Revue d'IFP Energies nouvelles 65 (6), 809–838.
Lacombe, O., Parlangeau, C., Beaudoin, N.E., Amrouch, K., 2021. Calcite twin formation, measurement and use as stress–strain indicators: a review of progress over the last decade. Geosciences 11 (11), 445.
Laurent, P., Kern, H., Lacombe, O., 2000. Determination of deviatoric stress tensors based on inversion of calcite twin data from experimentally deformed monophase samples. Part II. Axial and triaxial stress experiments. Tectonophysics 327 (1–2), 131–148.
Lavier, L., Steckler, M., Brigaud, F., 2001. Climatic and tectonic control on the Cenozoic evolution of the West African margin. Mar. Geol. 178, 63–80.
Lehner, P., De Ruiter, P.A.C., 1977. Structural history of the atlantic margin of Africa. AAPG (Am. Assoc. Pet. Geol.) Bull. 61 (7), 961–981.
Lentini, M.R., Fraser, S.I., Sumner, H.S., Davies, R.J., 2010. Geodynamics of the central South Atlantic conjugate margins: implications for hydrocarbon potential. Petrol. Geosci. 16 (3), 217–229.
Lundin, E.R., 1992. Thin-skinned extensional tectonics on a salt detachment, northern Kwanza Basin, Angola. Mar. Petrol. Geol. 9 (4), 405–411.
Machado, R., Roldan, L.F., Jacques, P.D., Fassbinder, E., Nummer, A.R., 2012. Tectônica transcorrente Mesozoica-Cenozoica no Domo de Lages-Santa Catarina. Rev. Bras. Geociencias 42, 799–811.
Mahatsente, R., Coblentz, D., 2015. Ridge-push force and the state of stress in the Nubia-Somalia plate system. Lithosphere 7 (5), 503–510.
Mahatsente, R., 2017. Global models of ridgeridge-push force, geoid, and lithospheric strength of oceanic plates. Pure Appl. Geophys. 174, 4395–4406.
Marton, L.G., Tari, G.C., Lehmann, C.T., Mohriak, W., 2000. Evolution of the Angolan passive margin, West Africa, with emphasis on post-salt structural styles. Geophysical Monograph-American Geophysical Union 115, 129–150.
Marzoli, A., Melluso, L., Morra, V., Renne, P.R., Sgrosso, I., D'Antonio, M., Duarte, Morais, L., Morais, E.A.A., Ricci, G., 1999. Geochronology and petrology of Cretaceous basaltic magmatism in the Kwanza Basin (western Angola) and relationships with the Parana-Edenteka continental flood basalt province. J. Geodyn. 28, 341–356.
Mastina, T., Zerbinati, A., 2021. Rock Mechanics Measurements on Cameia-1A and Cameia-3 Wells (TotalEnergies Unpublished internal report).
Matton, G., Jébrak, M., 2009. The Cretaceous Peri-Atlantic Alkaline Pulse (PAAP): deep mantle plume origin or shallow lithospheric break-up? Tectonophysics 469 (1–4), 1–12.
Mbina Mounguengui, M., Guiraud, M., 2009. Neocomian to early Aptian syn-rift evolution of the normal to oblique-rifted North Gabon margin (interior and N'Komi basins). Mar. Petrol. Geol. 26 (6), 1000–1017.
Medvedev, S., 2016. Understanding lithospheric stresses: systematic analysis of controlling mechanisms with applications to the African Plate. Geophys. J. Int. 207 (1), 393–413.
Mohriak, W., Nemčok, M., Enciso, G., 2008. South Atlantic divergent margin evolution: rift-border uplift and salt tectonics in the basins of SE Brazil. Geological Society 294 (1), 365–398. London, Special Publications.
Moulin, M., Aslanian, D., Olivet, J.L., Contrucci, I., Matias, L., Géli, L., Klingelhoefer, F., Nouzé, H., Unternehr, P., 2005. Geological constraints on the evolution of the Angolan margin based on reflection and refraction seismic data (ZaïAngo project). Geophys. J. Int. 162 (3), 793–810.
Moulin, M., Aslanian, D., Unternehr, P., 2010. A new starting point for the South and equatorial Atlantic Ocean. Earth Sci. Rev. 98 (1–2), 1–37.
Nkodia, H.V., Miyouna, T., Delvaux, D., Boudzoumou, F., 2020. Flower structures in sandstones of the Paleozoic Inkisi Group (Brazzaville, Republic of Congo): evidence for two major strike-slip fault systems and geodynamic implications. S. Afr. J. Geol. 123 (4), 531–550.
Nkodia, H.M.D.-V., Miyouna, T., Kolawole, F., Boudzoumou, F., Loemba, A.P.R., Bazebizonza Tchiguina, N.C., Delvaux, D., 2022. Seismogenic fault reactivation in western Central Africa: insights from regional stress analysis. G-cubed 23, e2022GC010377.

Nkodia, H.M.D., Boudzoumou, F., Miyouma, T., Kongota, E., Ganza, G.B., Lahogue, P., Delvaux, D., 2024. Brittle faulting and tectonic stress history on the western margin of the CongoBasin between Kinshasa and Brazzaville: implications for the evolution of the Malebo Pool and the Congo River. Tectonophysics 877, 230282.
Nurenberg, D., Müller, R.D., 1991. The tectonic evolution of the South atlantic from late jurassic to present. Tectonophysics 191 (1–2), 27–53.
Parlangeau, C., Lacombe, O., Schueller, S., Daniel, J.M., 2018. Inversion of calcite twin data for paleostress orientations and magnitudes: a new technique tested and calibrated on numerically-generated and natural data. Tectonophysics 722, 462–485.
Parlangeau, C., Dimanov, A., Lacombe, O., Hallais, S., Daniel, J.M., 2019. Uniaxial compression of calcite single crystals at room temperature: insights into twinning activation and development. Solid Earth 10 (1), 307–316.
Pascal, C., Cloetingh, S.A., 2009. Gravitational potential stresses and stress field of passive continental margins: insights from the south-Norway shelf. Earth Planet Sci. Lett. 277 (3–4), 464–473.
Pascal, C., 2006. On the role of heat flow, lithosphere thickness and lithosphere density on gravitational potential stresses. Tectonophysics 425, 83–99.
Passchier, C.W., Trouw, R.A.J., Ribeiro, A., Paciullo, F.V.P., 2002. Tectonic evolution of the southern Kaoko belt, Namibia. J. Afr. Earth Sci. 35, 61–75.
Pedrosa-Soares, A.C., Noce, C.M., Vidal, P., Monteiro, R.L.B.P., Leonardos, O.H., 1992. Toward a new tectonic model for the late proterozoic Araçuaí (SE Brazil)-West Congolian (SW Africa) belt. J. S. Am. Earth Sci. 6 (1–2), 33–47.
Perrier, R., Quiblier, J., 1974. Thickness changes in sedimentary layers during compaction history; methods for quantitative evaluation. AAPG Bull. 58 (3), 507–520.
Pichel, L.M., Legeay, E., Ringenbach, J., Callot, J., 2023. The West African salt-bearing rifted margin—regional structural variability and salt tectonics between Gabon and Namibe. Basin Research bre, 12796.
Pimienta, L., Fortin, J., Guéguen, Y., 2015. Experimental study of Young's modulusdispersion and attenuation in fully saturated sandstones. Geophysics 80 (5), 57–72.
Pletsch, T., Erbacher, J., Holbourn, A.E., Kuhnt, W., Moullade, M., Oboh-Ikuenobede, F. E., Söding, E., Wagner, T., 2001. Cretaceous separation of Africa and SouthSouth America: the view from the West African margin (ODP leg 159). J. S. Am. Earth Sci. 14 (2), 147–174.
Qiu, L., Chen, Z., Liu, Y., 2020. Recognition of the pre-salt regional structure of Kwanza basin, offshore in West Africa, derived from the satellite gravity data and seismic profiles. J. Geophys. Eng. 17, 956–966.
Quirk, D.G., Schødt, N., Lassen, B., Ings, S.J., Hsu, D., Hirsch, K.K., Von Nicolai, C., 2012. Salt tectonics on passive margins: examples from Santos, campos and Kwanza basins. Geological Society, London, Special Publications 363 (1), 207–244.
Rabinowitz, P.D., LaBrecque, J., 1979. The mesozoic South Atlantic ocean and evolution of its continental margins. J. Geophys. Res. Solid Earth 84 (B11), 5973–6002.
Riccomini, C., 1995. Padrão de fraturamentos do Maciço Alcalino de Cananéia, Estado de São Paulo: relações com a tectônica mesozóico-cenozóica do sudeste do Brasil. Rev. Bras. Geociencias 25, 79–84.
Roberts, N.M., Drost, K., Horstwood, M.S., Condon, D.J., Chew, D., Drake, H., et al., 2020. Laser ablation inductively coupled plasma mass spectrometry (LA-ICP-MS) U–Pb carbonate geochronology: strategies, progress, and limitations. Geochronology 2 (1), 33–61.
Roberts, N.M., Rasbury, E.T., Parrish, R.R., Smith, C.J., Horstwood, M.S., Condon, D.J., 2017. A calcite reference material for LA-ICP-MS U-Pb geochronology. G-cubed 18 (7), 2807–2814.
Rocher, M., Lacombe, O., Angelier, J., Chen, H.-W., 1996. Mechanical twin sets in calcite as markers of recent collisional events in a fold-and-thrust belt : evidence from the reefal limestones of southwestern Taiwan. Tectonics 15 (5), 984–996.
Rocher, M., Lacombe, O., Angelier, J., Deffontaines, B., Verdier, F., 2000. Cenozoic folding and faulting in the North Pyrenean Foreland (Aquitaine Basin, France): insights from combined structural and paleostress analyses. J. Struct. Geol. 22 (5), 627–645.
Rolland, A., Toussaint, R., Baud, P., Conil, N., Landrein, P., 2014. Morphological analysis of stylolites for paleostress estimation in limestones. Int. J. Rock Mech. Min. Sci. 67, 212–225.
Rouby, D., Raillard, S., Guillocheau, F., Bouroullec, R., Nalpas, T., 2002. Kinematics of a growth fault/raft system on the West African margin using 3-D restoration. J. Struct. Geol. 24 (4), 783–796.
Rowan, M.G., 2014. Passive-margin salt basins: hyperextension, evaporite deposition, and salt tectonics. Basin Res. 26 (1), 154–182.
Rowan, M.G., 2020. The South Atlantic and Gulf of Mexico salt basins: crustal thinning, subsidence and accommodation for salt and presalt strata. Geological Society, London, Special Publications 476 (1), 333–363.
Rowe, K.J., Rutter, E.H., 1990. Palaeostress estimation using calcite twinning: experimental calibration and application to nature. J. Struct. Geol. 12, 1–17.
Saller, A., Rushton, S., Buambua, L., Inman, K., McNeil, R., Dickson, J.A.D., 2016. Presalt stratigraphy and depositional systems in the Kwanza Basin, offshore Angola. AAPG (Am. Assoc. Pet. Geol.) Bull. 100 (7), 1135–1164.
Salomon, E., Koehn, D., Passchier, C., Hackspacher, P.C., Glasmacher, U.A., 2015. Contrasting stress fields on correlating margins of the South Atlantic. Gondwana Res. 28 (3), 1152–1167.
Schirbel, L., Assumpçao, M., Neto, F.A.P., França, G.S., 2024. Induced seismicity at the Lauca reservoir, Angola craton : focal mechanisms and implications for the stress field in Western Central Africa. J. Afr. Earth Sci. 216, 105327.
Schmittbuhl, J., Renard, F., Gratier, J.P., Toussaint, R., 2004. Roughness of stylolites: implications of 3D high resolution topography measurements. Phys. Rev. Lett. 93 (23), 238501.
Schoellkopf, N.B., Patterson, B.A., 2000. AAPG Memoir 73. Petroleum Systems of Offshore Cabinda, Angola (Chapter 25).
Séranne, M., Anka, Z., 2005. South Atlantic continental margins of Africa: a comparison of the tectonic vs climate interplay on the evolution of equatorial west Africa and SW Africa margins. J. Afr. Earth Sci. 43 (1–3), 283–300.
Szatmari, P., Milani, E.J., 2016. Tectonic control of the oil-rich large igneous-carbonate-salt province of the South Atlantic rift. Mar. Petrol. Geol. 77, 567–596.
Teboul, P.-A., 2017. Diagenesis of Lower Cretaceous Presalt Continental Carbonates from the West African Margin Simulations and Analogues. Aix- Marseille Université. Unpublished thesis.
Teisserenc, P., Villemin, J., 1989. Sedimentary basin of Gabon–geology and oil systems. In: Edwards, J.D., Santogrossi, P.A. (Eds.), Divergent/passive Margins Basins, 48. AAPG, pp. 117–199, 1990.
Torsvik, T.H., Rousse, S., Labails, C., Smethurst, M.A., 2009. A new scheme for the opening of the South Atlantic Ocean and the dissection of an Aptian salt basin. Geophys. J. Int. 177, 1315–1333.
Toussaint, R., Aharonov, E., Koehn, D., Gratier, J.P., Ebner, M., Baud, P., Rolland, A., Renard, F., 2018. Stylolites: a review. J. Struct. Geol. 114, 163–195.
Tullis, T.E., 1980. The use of mechanical twinning in minerals as a measure of shear stress magnitudes. J. Geophys. Res. Solid Earth 85 (B11), 6263–6268.
Turner, F.J., 1953. Nature and dynamic interpretation of deformation lamellae in calcite of three marbles. Am. J. Sci. 251, 276–298.
Turner, F.J., Griggs, D.T., Heard, H., 1954. Experimental deformation of calcite crystals. Geol. Soc. Am. Bull. 65 (9), 883–934.
Uncini, G., Brandao, M., Giovannelli, A., 1998. Neocomian-upper aptian pre-salt sequence of southern Kwanza Basin: a regional view. In: ABGP/AAPG International Conference and Exhibition November 8-11, 1998. Rio de Janeiro, Brazil.
Vagnes, E., Gabrielsen, R.H., Haremo, P., 1998. Late Cretaceous–Cenozoic intraplate contractional deformation at the Norwegian continental shelf: timing, magnitude and regional implications. Tectonophysics 300 (1–4), 29–46.
Viola, G., Andreoli, M., Ben-Avraham, Z., Stengel, I., Reshef, M., 2005. Offshore mud volcanoes and onland faulting in southwestern Africa: neotectonic implications and constraints on the regional stress field. Earth Planet Sci. Lett. 231, 147–160.
Viola, G., Kounov, A., Andreoli, M.A.G., Mattila, J., 2012. Brittle tectonic evolution along the western margin of South Africa: more than 500 Myr of continued reactivation. Tectonophysics 514, 93–114.
Wakamori, K., Yamaji, A., 2020. The integrated stress-strain analysis of calcite twins: consistent stress and strain determined from natural data. In: EGU General Assembly Conference Abstracts. European Geosciences Union, Vienna, 12819.
Wiens, D.A., Stein, S., 1983. Age dependence of oceanic intraplate seismicity and implications for lithospheric evolution. J. Geophys. Res. Solid Earth 88 (B8), 6455–6468.
Wiens, D.A., Stein, S., 1985. Implications of oceanic intraplate seismicity for plate stresses, driving forces and rheology. Tectonophysics 116 (1–2), 143–162.
Withjack, M.O., Olsen, P.E., Schlische, R.W., 1995. Tectonic evolution of the Fundy rift basin, Canada: evidence of extension and shortening during passive margin development. Tectonics 14 (2), 390–405.
Wonham, J.P., Cyrot, M., Nguyen, T., Louhouamou, J., Ruau, O., 2010. Integrated approach to geomodelling and dynamic simulation in a complex mixed siliciclastic–carbonate reservoir, N'Kossa field, Offshore Congo. Geological Society, London, Special Publications 347 (1), 133–163.
Woodhead, J.D., Hergt, J.M., 2001. Strontium, neodymium and lead isotope analyses of NIST glass certified reference materials: srm 610, 612, 614. Geostand. Newsl. 25 (2–3), 261–266.
Wright, K., Cygan, R.T., Slater, B., 2001. Structure of the (1014) surfaces of calcite, dolomite and magnesite under wet and dry conditions. Phys. Chem. Chem. Phys. 3, 839–844.
Zeboudj, A., Bah, B., Lacombe, O., Beaudoin, N.E., Gout, C., Godeau, N., Girard, J.-P., Deschamps, P., 2023. Depicting past stress history at passive margins: a combination of calcite twinning and stylolite roughness paleopiezometry in supra-salt Sendji deep carbonates, Lower Congo Basin, west Africa. Mar. Petrol. Geol. 152, 106219.
Ziegler, P.A., Cloetingh, S., van Wees, J.D., 1995. Dynamics of intra-plate compressional deformation: the Alpine foreland and other examples. Tectonophysics 252 (1–4), 7–59.